AGU PUBLICATIONS

JGR

Journal of Geophysical Research: Planets

RESEARCH ARTICLE
10.1002/2017JE005283

Key Points:
- Transient crater scaling relationships are derived over a large range of target properties for simple craters
- The effects of the coefficient of friction and porosity are successfully included in the existing π group scaling law
- Compaction model parameters other than the initial porosity influence transient crater diameter only for porosity smaller than 10–15%

Supporting Information:
- Supporting Information S1
- Data Set S1

Correspondence to:
N. C. Prieur,
nilscp@geo.uio.no

Citation:
Prieur, N. C., T. Rolf, R. Luther, K. Wünnemann, Z. Xiao, and S. C. Werner (2017), The effect of target properties on transient crater scaling for simple craters, *J. Geophys. Res. Planets*, *122*, 1704–1726, doi:10.1002/2017JE005283.

Received 10 FEB 2017
Accepted 18 JUL 2017
Accepted article online 20 JUL 2017
Published online 13 AUG 2017

The effect of target properties on transient crater scaling for simple craters

N. C. Prieur[1], T. Rolf[1], R. Luther[2], K. Wünnemann[2,3], Z. Xiao[1,4,5], and S. C. Werner[1]

[1]Centre for Earth Evolution and Dynamics, University of Oslo, Oslo, Norway, [2]Museum für Naturkunde, Leibniz-Institute for Evolution and Biodiversity Science, Berlin, Germany, [3]Institute of Geological Sciences, Planetary Sciences and Remote Sensing, Freie Universität Berlin, Berlin, Germany, [4]Planetary Science Institute, School of Earth Sciences, China University of Geosciences, Wuhan, China, [5]Space Science Institute, Macau University of Science and Technology, Macau, China

Abstract The effects of the coefficient of friction and porosity on impact cratering are not sufficiently considered in scaling laws that predict the crater size from a known impactor size, velocity, and mass. We carried out a systematic numerical study employing more than 1000 two-dimensional models of simple crater formation under lunar conditions in targets with varying properties. A simple numerical setup is used where targets are approximated as granular or brecciated materials, and any compression of porous materials results in permanent compaction. The results are found to be consistent with impact laboratory experiments for water, low-strength and low-porosity materials (e.g., wet sand), and sands. Using this assumption, we found that both the friction coefficient and porosity are important for estimating transient crater diameters as is the strength term in crater scaling laws, i.e., the effective strength. The effects of porosity and friction coefficient on impact cratering were parameterized and incorporated into π group scaling laws, and predict transient crater diameters within an accuracy of ±5% for targets with friction coefficients $f \geq 0.4$ and porosities $\Phi = 0$–30%. Moreover, 90 crater scaling relationships are made available and can be used to estimate transient crater diameters on various terrains and geological units with different coefficient of friction, porosity, and cohesion. The derived relationships are most robust for targets with $\Phi > 10$–15%, applicable for a lunar environment, and could therefore yield significant insights into the influence of target properties on cratering statistics.

1. Introduction

Target properties have been found to substantially influence impact crater evolution. However, crater scaling relationships have only been derived for a few combinations of target properties such as dry and wet sand as well as water targets [*Holsapple and Schmidt*, 1982; *Schmidt and Housen*, 1987; *Holsapple and Housen*, 2007]. Scaling relationships with target properties similar to lunar materials such as basalts, feldspathic highland crust, and impact basin ejecta are not yet available. This strongly limits the applicability of existing crater scaling laws to quantify the influence of target properties on terrains with varying geology [*Fassett*, 2016]. The purpose of this paper is to systematically assess the influence of the coefficient of friction, porosity, and cohesion (i.e., the shear strength at zero pressure, section 4.1) on diameters of transient craters. Existing π group scaling laws relating transient crater diameter to impactor and target properties [*Buckingham*, 1914; *Holsapple and Schmidt*, 1987; *Holsapple*, 1993] are used to fit results of numerical models under lunar conditions. The outcome of this study provides scaling relationships for a wide range of target properties and advances our understanding of the impact cratering process by integrating more diverse target properties into crater scaling laws.

The size of a crater that results from an impact of given size is well described by power laws [*Holsapple and Schmidt*, 1987]. Over the last decades, experimental studies on various targets such as metals [e.g., *Dienes and Walsh*, 1970], water [e.g., *Gault and Sonett*, 1982; *Schmidt and Housen*, 1987], dry and wet sand [e.g., *Gault and Wedekind*, 1977; *Piekutowski*, 1977; *Schmidt*, 1980; *Holsapple and Schmidt*, 1982; *Schmidt and Housen*, 1987; *Yamamoto et al.*, 2006], and rocks [e.g., *Moore et al.*, 1963; *Gault*, 1973; *Poelchau et al.*, 2013] proved the applicability of this power law description but also revealed that target properties influence the crater scaling relationships. However, a comprehensive understanding of the effects of target properties on crater sizes is still lacking. Experimental approaches face several limitations such as the dependency of target properties upon each other (e.g., density and porosity), which makes it difficult to constrain the sole effect of a specific property on crater dimensions [*Housen and Holsapple*, 2003; *Housen and Holsapple*, 2011].

Thus, experimentally derived crater relationships to date cannot account for variations induced by target properties such as the coefficient of friction and porosity [*Elbeshausen et al*., 2009].

In contrast, numerical calculations provide a tool for systematic investigation of individual target properties over a wide range of values and allow to extend the study of cratering dynamics to planetary scale [*Pierazzo and Collins*, 2004]. The numerical approach has been widely used in the past to assess the role of projectile and target properties such as the effect of the coefficient of friction [*Elbeshausen et al*., 2009; *Wünnemann et al*., 2011], porosity [*Wünnemann et al*., 2006; *Collins et al*., 2011; *Wünnemann et al*., 2011], and cohesion [*O'Keefe and Ahrens*, 1993; *Wünnemann et al*., 2011; *Güldemeister et al*., 2015] on crater growth.

Generally, crater size is mostly influenced by three main target properties, namely, the friction coefficient, porosity, and cohesion [*Housen and Holsapple*, 2011]. The effect of the coefficient of friction (hereafter denoted as *f*) on craters was first discussed by *Holsapple and Schmidt* [1979] and *Schmidt* [1980]. Their study shows that an increase of *f* decreases the crater diameter. Recently, *Elbeshausen et al*. [2009] and *Wünnemann et al*. [2011] investigated the effect of *f* on crater diameters by numerical modeling of crater formation. Their results showed a good agreement with experimental studies [*Schmidt*, 1980] and underlined possible relationships between derived scaling parameters and *f*. The effect of target porosity has been addressed in several experimental studies [*Love et al*., 1993; *Housen*, 1999; *Housen and Holsapple*, 2003]. These studies confirm that through compaction of pores, a large amount of energy is dissipated [e.g., *Zel'Dovich and Raizer*, 1966]. This may result in deeper craters [e.g., *Love et al*., 1993]; increased heating and melting of the target [e.g., *Kieffer*, 1975; *Wünnemann et al*., 2008]; faster decay of the impact-induced shock wave [e.g., *Zel'Dovich and Raizer*, 1966; *Pierazzo*, 1997]; reduction of the amount, speed, and angles at which material is ejected [e.g., *Housen and Holsapple*, 2003; *Housen and Holsapple*, 2011]; and for this study most importantly decrease of the crater diameter [*Wünnemann et al*., 2006; *Collins et al*., 2011; *Wünnemann et al*., 2011]. These studies underlined the importance of the coefficient of friction and porosity; however, no further effort has been made to include their effects in crater scaling laws. For competent rocks and for small impact craters, the cohesive strength plays an important role [*Holsapple and Schmidt*, 1979]. Although target strength is already included in existing π-scaling laws, the actual meaning of the strength term is not very well defined and different strength characteristics such as tensile, compressive, and shear strengths have been used to describe the effect of the resistance of material against deformation on crater size [*Housen and Holsapple*, 2011]. To match experimental [*Poelchau et al*., 2013] and numerical results [*Güldemeister et al*., 2015] for sandstone and quartzite targets, the effective strength (i.e., the strength parameter in crater scaling laws, section 3) could be up to 5 orders of magnitude below the uniaxial compressive material strength. However, further work is required to understand these discrepancies and to define an appropriate strength parameter in crater scaling laws.

A clear understanding of how target properties affect the impact process is thus essential in numerous aspects of planetary geology. These effects may be particularly important when using populations of small craters to date small areas of and/or young geological units for which the importance of target properties has not been sufficiently considered yet [*Schultz and Spencer*, 1979; *Dundas et al*., 2010; *Fassett*, 2016; *van der Bogert et al*., 2016].

In the remainder of this paper, we describe the basics of impact crater mechanics and scaling laws (sections 2 and 3). A description of the numerical model setup and a comparison of results against experimental studies are given in section 4. Results are presented in section 5. The incorporation of the coefficient of friction and porosity in the π group scaling law, model limitations, and a discussion of the results are presented in sections 6 and 7, respectively. Finally a concluding summary is presented in section 8.

2. Crater Formation and Transient Crater

To separate different processes governing crater formation as a function of time and space, it is convenient to subdivide impact crater formation into three stages [*Melosh*, 1989]. First, during the contact and compression stage the impact of a projectile on a target generates a shock wave at the contact zone, which propagates through the target, transferring much of the kinetic energy of the impactor to the target. As a consequence of shock compression and subsequent shock wave release, material is set into motion, which results in the excavation of a deep bowl-shaped crater (excavation stage). The growth of the crater cavity stops when the residual kinetic energy of the target is insufficient to displace the target against its own weight

(gravity-dominated cratering) or against the material strength (strength-dominated cratering). At the end of this stage, the crater is often called the transient crater [*Dence*, 1968]. Subsequently, the transient crater collapses to form the final crater (modification stage). Depending on the size of the transient crater and the degree of subsequent collapse during modification, crater morphologies observed on planetary surfaces are generally classified into two groups: (1) bowl-shaped simple craters and (2) complex craters that feature a combination of crater terraces, central uplift, and multiring structures [*Melosh and Ivanov*, 1999].

Due to the distinction between the transient crater and final crater, it also makes sense to quantify crater formation by a two-step approach: the formation of the transient crater and the collapse (resulting in a final crater). Studying crater evolution until final crater formation requires models to include the whole modification stage, which increases computational time substantially. Alternatively, transient craters (1) are reached earlier during crater formation, (2) are the best measure of the kinetic energy transmitted from the projectile to the target [e.g., *Schmidt and Housen*, 1987], and (3) have diameters that are well described by power laws [e.g., *Holsapple*, 1993]. Therefore, the use of transient crater geometries facilitates the development of robust crater-to-projectile scaling relationships and further allows separation of the influence of target properties from other processes. Therefore, we focus on scaling relationships derived for transient crater diameters for simple craters; relationships for the final rim-to-rim crater diameters are not addressed here yet.

The definition of the transient crater is a crucial step in the development of robust crater scaling relationships from numerical experiments. Typically, it is defined as the maximum extent to which excavation proceeds in every direction [e.g., *Dence*, 1968; *Turtle et al*., 2005; *Elbeshausen et al*., 2009; *Wünnemann et al*., 2011]. However, the definition of transient crater is subtle because the maximum geometric extent of the cavity is reached at different times for different components (e.g., diameter and depth) during crater growth [*Turtle et al*., 2005; *Elbeshausen et al*., 2009]. In previous studies the transient crater was not defined as its maximum extent but at the time when it reached either its maximum depth [e.g., *Elbeshausen et al*., 2009] or volume [e.g., *Elbeshausen et al*., 2009; *Güldemeister et al*., 2015]. Although not exact, the definition of transient crater at a specific time is expected to be reasonable for laboratory experiments, where the amount of collapse is minimal and the excavation flow relatively simple (i.e., crater growth first ceases to expand vertically, and then horizontally). However, this assumption might not be applicable for impact crater on planetary scale. *Turtle et al*. [2005] discussed the challenges in defining a transient crater for complex craters. The rapid uplift of the crater floor causes a relatively complex evolution of the crater, where both the excavation (horizontally) and modification (crater floor uplift) stages occur simultaneously. Because of possible dependencies of scaling relationships for complex craters on the definition of the transient crater, the present study focuses on simple craters, i.e., crater diameters less than 16–19 km on the Moon [*Pike*, 1980]. The influence of the transient crater definition on the derived scaling results is investigated in the supporting information (for details, see Text S1). We chose to define the transient crater diameter to be the diameter of the crater at the time of maximum cavity volume, because it gave the most consistent results with experimental studies.

3. Crater Scaling Laws

Although projectile size and velocity associated with a crater observed on a planetary surface are unknown, we can use empirical relationships (crater scaling laws) to predict crater sizes from known impactor and target properties. To estimate the outcome of an impact, crater scaling laws employ the point source approximation as initial impact condition in which the projectile's energy and momentum are released in a small region, the so-called coupling zone, buried at a certain depth in the target [*Holsapple and Schmidt*, 1987]. According to this concept, a number of impact-related processes (e.g., shock wave decay, ejection, and crater formation) observed at a late stage during crater formation can be described by a single coupling parameter C (equation (1)) that depends on the initial impactor (diameter L, density δ, and velocity U) and target properties [*Dienes and Walsh*, 1970; *Holsapple and Schmidt*, 1987],

$$C = LU^{\mu}\delta^{\nu}. \tag{1}$$

In this late-stage process, C is proportional to a combination of the energy and the momentum of the impactor and is quantified by the velocity-scaling exponent μ, while ν is the density scaling exponent.

The most common and successful approach to predict crater size for a given impact is the so-called π group scaling. A detailed description is given in *Holsapple and Schmidt* [1982, 1987] and *Holsapple* [1993]. Only a summary for the determination of the transient crater diameter D as a function of projectile and target properties (density ρ, gravity g, and effective strength Y_{EFF}) is stated here:

$$D = f_1(U, L, \delta, \rho, Y_{\mathrm{EFF}}, g). \tag{2}$$

To decrease the number of parameters, the independent variables are gathered into dimensionless groups [*Buckingham*, 1914]. The dimensionless analysis of equation (2) yields

$$\pi_D = f_2(\pi_2, \pi_3, \pi_4), \tag{3}$$

with the dimensionless crater diameter π_D and

$$\pi_2 = 1.61\,\frac{gL}{U^2}, \tag{4}$$

$$\pi_3 = \frac{Y_{\mathrm{EFF}}}{\rho U^2}, \tag{5}$$

$$\pi_4 = \frac{\rho}{\delta}. \tag{6}$$

The gravity-scaled size π_2 is the ratio of gravitational and inertial stresses and indicates the importance of gravity limiting the size of the transient crater (equation (4)). The parameter π_3 is the strength-scaled size, a measure of the importance of target material strength in stopping crater growth (equation (5)). The effective strength Y_{EFF} encompasses a large number of processes and properties that influence the overall strength of the target during crater growth [*Holsapple*, 1993]. Whether this parameter is related to any specific measure of material strength or numerical strength model parameter is not yet understood (see section 4.1). Finally, π_4 denotes the ratio of target and projectile densities (equation (6)). The use of dimensionless parameters makes it possible to relate small-scale experiments with various impact velocities, projectile sizes, and target properties to large-scale natural craters in different gravity environments [*Holsapple and Schmidt*, 1982].

The dimensionless crater diameter (π_D) is proportional to the ratio of the transient crater diameter and the projectile diameter. The parameter π_D provides insight into the efficiency to open the crater cavity while also considering the density contrast of projectile and target [e.g., *Schmidt*, 1980]:

$$\pi_D = D\left(\frac{\rho}{m_i}\right)^{\frac{1}{3}}, \tag{7}$$

where m_i is the mass of the projectile.

The parameter π_D can be expressed in terms of dimensionless parameters and scaling coefficient (K_1) and exponents (μ and ν). In its complete form, a single crater scaling law covers both the strength and gravity regime [*Holsapple*, 1993]:

$$\pi_D = K_1\left[\pi_2\,\pi_4^{\frac{2+\mu-6\nu}{-3\mu}} + \left(\pi_3\,\pi_4^{\frac{2-6\nu}{-3\mu}}\right)^{\frac{2+\mu}{2}}\right]^{\frac{-\mu}{2+\mu}}. \tag{8}$$

Note that the scaling coefficient K_2 is here included in the effective strength parameter Y_{EFF} and the strength-scaled size (equation (5)) following *Holsapple* [1993]. As an example, Figure 1 shows schematically π_D as a function of π_2 (equation (8)) for two materials with similar coefficient of friction and porosity. Material 1 (M1) is a typical example for the behavior of granular materials with no effective strength in the absence of overburden pressure ($Y_{\mathrm{EFF}} = 0$ and $\pi_3 = 0$), whereas material 2 (M2) has a finite effective strength such as rocks ($Y_{\mathrm{EFF}} \neq 0$ and $\pi_3 \neq 0$). For sufficiently small π_2, the π_3 term in equation (8) dominates and the scaled crater diameter becomes independent of the gravity-scaled size π_2. In this case, crater size is controlled by strength (strength-dominated crater) and equation (8) simplifies to

$$\begin{aligned} &\pi_D = K_1 {\pi_3}^{\frac{-\mu}{2}} {\pi_4}^{\frac{-\mu}{3}}, \\ &\pi_D = K_{DS} {\pi_3}^{-\varsigma}, \text{with } K_{DS} = K_1 {\pi_4}^{\frac{1-3\nu}{3}} \text{ and } \varsigma = \frac{-\mu}{2}. \end{aligned} \tag{9}$$

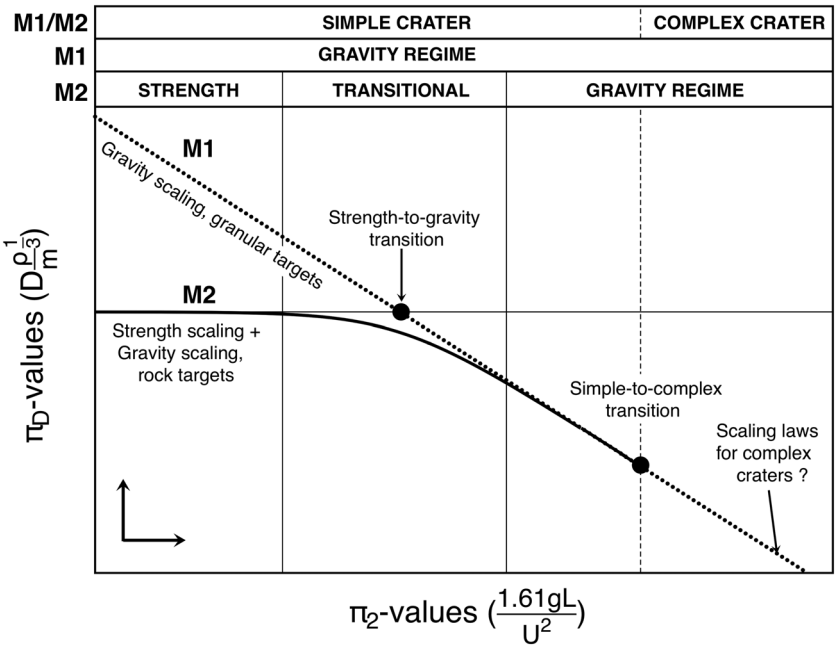

Figure 1. Dimensionless crater diameter (π_D) as a function of the gravity-scaled size (π_2). Schematic description of typical scaling laws for granular (M1, dotted line) and rock (M2, bold line) target materials. The different crater formation regimes for M1 and M2 are labeled at the top of the diagram. The thin, vertical dashed line represents the simple-to-complex transition. Note that this schematic description is similar to Figure 18 in *Neukum and Ivanov* [1994].

For larger craters (i.e., larger π_2 values) or for granular targets ($Y_{EFF} = 0$ and $\pi_3 = 0$), gravity dominates ($\pi_2 \gg \pi_3$), and the effects of cohesion can be neglected. The scaling line for material M2 converges toward the granular material M1 and the gravity scaling. In this regime, an increase in π_2 results in a decrease in π_D following a simple power law line (dotted line in Figure 1) and equation (8) simplifies to

$$\pi_D = K_1 {\pi_2}^{\frac{-\mu}{2+\mu}} {\pi_4}^{\frac{2+\mu-6\nu}{3(2+\mu)}},$$
$$\pi_D = K_D {\pi_2}^{-\beta}, \text{with } K_D = K_1 {\pi_4}^{\frac{2+\mu-6\nu}{3(2+\mu)}} \text{ and } \beta = \frac{\mu}{2+\mu}. \quad (10)$$

The scaling parameters K_1, μ, and ν (equations (8)–(10)) can be determined empirically by laboratory cratering or numerical experiments by fitting either equation (9) for strength-dominated craters or equation (10) for gravity-dominated craters to the experimental or numerical data. Because the transition from purely gravity-dominated craters to purely strength-dominated craters is gradual, data from the transition regime has to be cautiously excluded, when equation (9) or (10) is used to determine the scaling parameters [e.g., *Güldemeister et al.*, 2015]. The crater diameter at which this transition occurs is often referred to as the strength-to-gravity transition D_{SG} [see *Croft*, 1985, Figure 1]. This transition is here defined as the point where the horizontal interpolation of the strength regime intersects with the gravity scaling [*Neukum and Ivanov*, 1994] (Figure 1).

The scaling laws provide two important pieces of information. First, they indicate how D (π_D) varies in different targets as a function of projectile size, velocity, mass, gravity (π_2), and strength (π_3). Second, the velocity exponent (μ) expresses the proportionality of the crater size to the projectile energy and momentum. If the crater size is proportional to the impact energy, $\mu = 2/3$, whereas $\mu = 1/3$ if it scales with the momentum of the impactor [*Holsapple and Schmidt*, 1987]. Therefore, μ is bounded by two theoretical end-member values and depends on target properties such as the coefficient of friction and porosity [*Schmidt*, 1980; *Holsapple and Schmidt*, 1987]. In general, craters that scale close to the energy limit form in materials with little (or no) initial porosity or friction coefficient, whereas craters that scale closer to the momentum limit form in materials with significant initial porosity and friction coefficient, such as sand.

According to the π-scaling and late-stage equivalence concepts [*Holsapple and Schmidt*, 1982; *Schmidt and Housen*, 1987; *Holsapple*, 1993], μ is a material-specific constant and crater size depends on impact velocity only through the π_2 and π_3 terms (i.e., there is no other dependence on impact velocity). Under this assumption, μ can

be determined from the power law relationship between scaled crater size (e.g., π_D) and scaled source size (e.g., π_2), regardless of which independent variable (e.g., impact velocity U, impactor diameter L, or gravity g) is varied. We adopt this assumption here and vary π_2 in our numerical simulations by varying only the impactor diameter and fixing the target gravity and impact velocity. We note that if there is any additional impact velocity dependence to crater scaling, contrary to the assumption made here, the scaling laws that stem from our results would apply only for impacts at speeds similar to that used in our study (12.7 km/s). In particular, it is possible that an additional velocity dependence applies for impact speeds lower than the target sound speed [e.g., *Housen and Holsapple*, 2011; *Yamamoto et al*., 2017], and so our results should be applied with caution in this regime. Finally, the density scaling exponent is kept constant here ($\nu = 0.4$), which corresponds to a reasonable value for a wide range of materials and is estimated from previous experimental studies [e.g., *Holsapple*, 1993].

4. Numerical Experiments

4.1. Model Setup

We compute impact crater formation using the iSALE-2D shock physics code (iSALE-Chicxulub, www.isale-code.de), which is based on the SALE hydrocode solution algorithm [*Amsden et al*., 1980]. Recent modifications include a sophisticated strength model [*Collins et al*., 2004], a porosity compaction model [*Wünnemann et al*., 2006; *Collins et al*., 2011], a dilatancy model [*Collins*, 2014], and various equations of state, and the code can simulate impacts into multiple materials [*Melosh et al*., 1992; *Ivanov et al*., 1997]. iSALE-2D has been rigorously validated against experimental studies [*Pierazzo et al*., 2008; *Davison et al*., 2011; *Miljković et al*., 2012] and is therefore an adequate tool for this study.

Because of the 2-D setup, we are limited to vertical (90°) impacts. Simulations are conducted for a lunar surface (g = 1.62 m/s^2) with a constant impact velocity of U = 12.7 km/s, which is the vertical component of the average lunar impact velocity (18 km/s) at a 45° angle [e.g., *Ivanov*, 2001; *Elbeshausen et al*., 2009]. For each target, projectile diameters are varied (25 m $\leq L \leq$ 1000 m) and only craters resulting in simple craters are selected for further analyses. The transient crater is defined in our models at the maximum cavity volume (section 2 and supporting information Text S1) and the transient diameter measured at the preimpact surface.

We use the Drucker-Prager model to describe the mechanical behavior of target materials. This strength model defines the shear strength of the bulk material, Y, as $Y = \min(Y_0 + fp; Y_{LIM})$, where Y_0 is the strength at zero pressure (the cohesion), p is the overburden lithostatic pressure, Y_{LIM} is the limiting strength at high pressure, and f is the coefficient of internal friction (which controls the change of strength with pressure). As described in detail in *Elbeshausen et al*. [2009], the coefficient of friction in iSALE f does not exactly match the coefficient of friction in a Mohr-Coulomb model f_{mc}. However, f and f_{mc} can be approximately related by $f \approx f_{mc}\cos\theta$, where the angle of internal friction $\theta = \tan^{-1} f_{mc}$. Note that f and f_{mc} are not uniquely related, because f depends on all three principle stresses (σ_1, σ_2, and σ_3), while the Mohr-Coulomb model assumes $\sigma_2 = \sigma_3$. The Drucker-Prager model best represents the behavior of granular materials. We also use it here for rock targets, which is a simplification since strength degradation owing to fracturing is neglected [*Collins et al*., 2004]. However, we point out that as a consequence of the passage of the shock wave and subsequent release wave, rocks in the vicinity of the crater are heavily shattered. Therefore, the combination of continuous bombardment of a surface coupled with fragmentation due to impact cratering is likely to result in old surfaces that become extensively fractured and fragmented over time. The crater growth occurs in the fractured (damaged) zone, where the material may be considered as granular or breccia. The use of a more complex strength model [*Collins et al*., 2004] requires at least twice as many parameters, which would make systematic investigation more realistic but also more complicated. The effect of Y_{LIM}, the limiting strength at high pressure, is investigated in detail in section 5.2. The shear strength of the material depends also on the target's preimpact temperature and pressure as well as the melting temperature of the material. If temperature exceeds the melting point, the shear strength drops to zero [*Collins et al*., 2004]. In iSALE-2D, this thermal softening is accounted for by using the formulation of *Ohnaka* [1995].

The targets in our models consist of a single basalt layer without any spatial variations (half space). The projectile is composed of nonporous basalt in all models. The analytical tabulated equation of state (ANEOS) for basalt [*Pierazzo et al*., 2005] is used to describe the thermodynamic state of the projectile and the target material.

We investigate the effect of target porosity with the help of the ε-α compaction model [*Wünnemann et al*., 2006; *Collins et al*., 2011] in which collapse of pore spaces is described by a compaction function relating

the porosity and the volumetric strain (pressure). The porosity model requires five input parameters each of which has a physical meaning (α_0, α_x, K, ε_e, and χ). The parameter α_0 is the initial distension and is related to the porosity with $\alpha = 1/(1 - \Phi)$. The parameter α_x is the distension at the transition that separates two regimes, i.e., the compaction due to grain rearrangement (exponential decay) and fracturing of individual grains (power law decay). K is the compaction rate in the exponential compaction regime, ε_e is the volumetric strain at the onset of plastic (irreversible) compaction, and χ is the ratio between the porous and nonporous bulk sound speed. To reduce the number of free model parameters, the compaction model parameters are here held constant regardless of the initial porosity in the target. Ideally, each of these model parameters would be determined from specific crushing experiments for a given material and these parameters may vary depending on the initial porosity [e.g., *Wünnemann et al*., 2006; *Davison et al*., 2010; *Collins et al*., 2011; *Miljković et al*., 2012]. However, such experiments are only available for a limited number of materials that are not representative for the lunar surface and upper crust. For this study, we use $\varepsilon_e = 0$, $\kappa = 0.98$, $\alpha_x = 1.0$, and $\chi = 1$ in all cases. These parameter values have been shown to approximate targets with moderate porosity such as sands reasonably well [*Wünnemann et al*., 2006; *Collins et al*., 2011]. To test whether the assumption of holding compaction parameters constant is valid over a larger range of porosity, a sensitivity analysis of scaling results on compaction model parameters is conducted in section 5.2. The implications of the simplifications related to the strength and compaction models are discussed in section 7.1.

A model to account for dilatancy (the increase in porosity as a consequence of shear deformation) is available in iSALE [*Collins*, 2014] but is not used here because we consider only transient crater formation. *Collins* [2014] showed that dilatancy is most important during the modification stage and that transient crater size is relatively insensitive to dilatancy. A resolution of 20 cells per projectile radius provides the best compromise between reasonable computation time and sufficient accuracy (see supporting information Text S2). All cases use a high-resolution zone at least 1.5–2 times larger than the expected transient craters and a surrounding extensional zone (i.e., a zone where the cell size is gradually increased) to minimize the possible effects of shock wave reflections at the models' boundaries [e.g., *Wünnemann et al*., 2011]. Target properties such as the coefficient of friction, porosity, and cohesion are varied one at a time in order to isolate and understand their influence on transient crater diameters. Target properties and model parameters are summarized in Tables 1 and 2.

4.2. Comparison With Existing Scaling Relationships

For all cases the thermodynamic state of the target material is described by the equation of state for basalt together with the ε-α porosity model, regardless of the nature of the material. The water target is, for instance, approximated as a strengthless basalt ($f = 0$ and $Y_0 = 0$), whereas sand is approximated by a "basaltic" sand with similar physical properties as sand. Even though simplified, this systematic approach contributes to a better understanding of the effect of material properties on lunar crater formation. To assess the reliability of the numerically derived scaling results, we compare them with established scaling laws that are based on physical cratering experiments for different types of sand materials and water (Figure 2). Experimentally derived crater relationships are based on final crater diameters. But because of the small degree (i.e., ~10% differences between the transient and final crater diameters, both measured from the preimpact surface) of final crater collapse in experiments [e.g., *Ormö et al*., 2015; *Wünnemann et al*., 2016], these crater relationships are comparable with our numerical results derived from transient crater diameters. When available, the friction coefficient and porosity values were taken from references specified in Table 3. Wet sand may have a very small internal coefficient of friction, close to the zero internal coefficient of friction of water [*Wünnemann et al*., 2006; *Elbeshausen et al*., 2009]. A coefficient of friction of 0.1 (and an uncertainty value of 0.1) was therefore used as a representative value.

In general, our results agree very well with experimental results (Figure 2), which indicates the validity of the above described model setup and proves that this model can be used over a wide range of target properties such as those for the materials presented in Table 3. The experimental scaling relationship for dry sand (i.e., dense and loose sands) falls in between our numerical scaling lines for $f = 0.6$–0.8 and $\Phi = 30$–40% (Figure 2b). Results are thus in good agreement with typical coefficients of friction ($f = 0.7$) [*Elbeshausen et al*., 2009; *Miljković et al*., 2012] and porosities ($\Phi = 30$–40%) for sand [*Holsapple and Schmidt*, 1982]. The derived scaling exponents (β) differ by less than 1% from experimental data (Table 3), while the scaling coefficients (K_D) match reasonably (~ ± 10%). This is also supported by direct comparison of the experimentally and numerically derived scaling relations, which generally deviate by only 5% or less (Figure 2c).

Table 1. Model Parameters Used in the Analysis of Impact Cratering Solely Governed by Gravity (Under Lunar Conditions and Size of Projectiles Used in This Study)

Parameters	Symbol	Value(s) Employed	Unit
Equation of state	-	ANEOS Basalt	-
Poisson's ratio	-	0.25	-
Global setup parameters			
Impact velocity	U	12.7	km/s
Gravitational acceleration	g	1.62	m/s^2
Thermal parameters			
Solidus (at zero pressure)	-	1360	K
Specific heat capacity	-	850	J/kg/K
Thermal softening parameter	-	1.2	-
Constant in Simon's approximation (Pa)	-	4.5×10^9	Pa
Exponent in Simon's approximation (−)	-	3.0	-
Thermal gradient (K/km)	-	3.0	K/km
Strength parameters			
Cohesion of material	Y_0	5	Pa
Coefficient of internal friction	f	0.0, 0.1, 0.2, 0.4, 0.6, 0.8, 0.9, 1.0	-
Limiting strength at high pressure	Y_{LIM}	1.0×10^9	Pa
Porosity properties			
Initial porosity	Φ	0, 1, 2, 3, 5, 6, 8, 9, 10, 12, 20, 30, 40, 50	%
Elastic threshold	ε_e	0.0	-
Transition from power to exp. decay	α_X	1.0	-
Kappa—exponential coefficient	κ	0.98	-
Sound speed ratio	χ	1.0	-

Based on the high degree of similarity of scaling relationships for geological materials and the numerical analogs used here, we find that (1) our scaling laws for cohesionless granular materials can be extrapolated down to laboratory scale ($\pi_2 \sim 10^{-8}$–10^{-9}), (2) crater mechanisms for simple craters are comparable to laboratory-scale experiments, and (3) natural materials can be reasonably approximated by a target with a constant equation of state for basalt and similar properties.

5. Results

Crater scaling laws in the gravity and strength regime have a distinct behavior (Figure 1). Therefore, we separated our study into two sets of experiments. First, we studied granular targets, here defined as targets with negligible cohesive strength (often denoted as cohesionless, $Y_0 = 0$), to derive scaling laws purely in the gravity regime. Note that the term cohesionless ($Y_0 = 0, f \neq 0$) is different from the term strengthless ($Y_0 = f = 0$). For these experiments, only friction coefficient (f) and porosity (Φ) are varied (Table 1). Second, we investigated the effect of target properties on rock-like materials (often denoted as competent materials, $Y_0 \neq 0$), i.e., here simulated as brecciated materials with large cohesive strength, high coefficient of friction, and low porosity

Table 2. Model Parameters Used in the Analysis of Impact Cratering Governed by Both Gravity and Material Strength[a]

Parameter	Symbol	Value(s) Employed	Unit
Impact velocity	U	12.7	km/s
Gravitational acceleration	g	1.62	m/s^2
Coefficient of internal friction	f	0.2, 0.4, 0.6, 0.8	-
Initial porosity	Φ	10, 20, 30, 40	%
Cohesion of material	Y_0	0.05, 0.1, 0.5, 1.0, 2.0, 5.0, 10.0	MPa

[a]Note that only some of the possible combinations of parameters were modeled. The parameter space covered here is much smaller than in Table 1 due to the fact that three target properties are now systematically varied, increasing considerably the number of possible combinations.

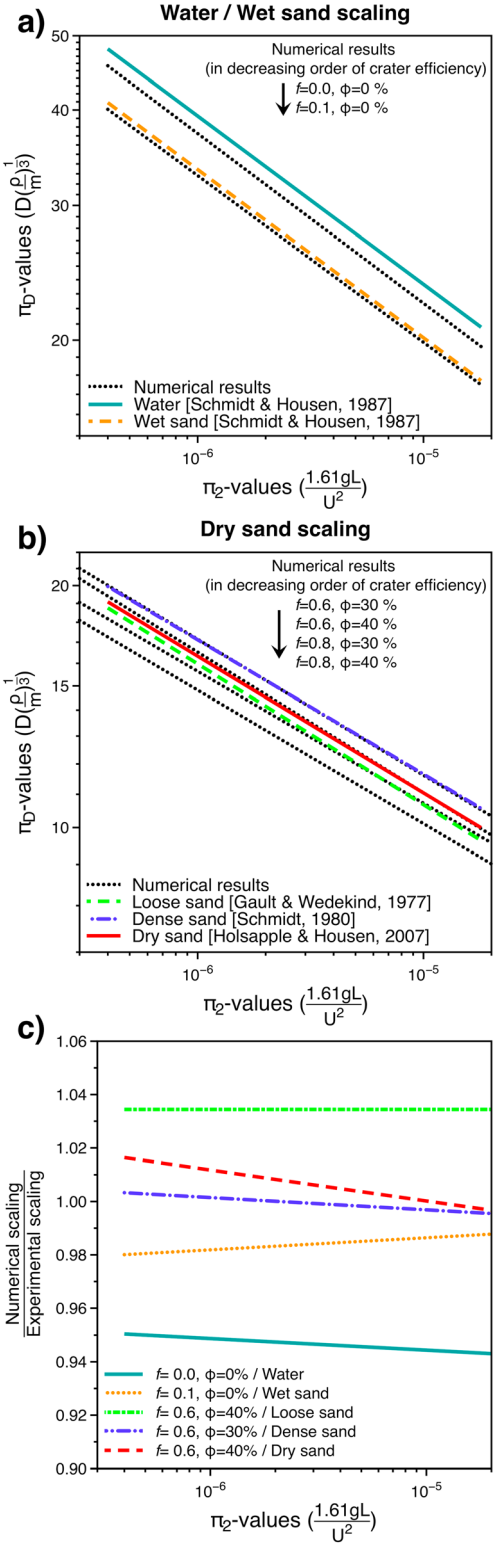

Figure 2. The π scaling for experimentally (colored bold lines) and numerically derived (black dots) for (a) water and wet-sand targets and (b) for different types of dry sand materials (see Table 3). (c) Ratios of numerical and experimental results for similar target properties.

(see section 4.1). Crater scaling laws are derived for several combinations of target properties (see Table 2) and relationships between friction coefficient, porosity, and cohesion of the material and scaling parameters are evaluated.

5.1. The Effect of the Coefficient of Friction and Porosity on Transient Crater Diameter for Gravity-Dominated Craters

We performed 30 simulations with varying coefficients of friction (f = 0.1, 0.2, 0.4, 0.8) to investigate the effect of friction coefficient on transient crater diameter for porous targets (using a constant porosity of Φ = 30%, Figure 3a). For each combination of target properties, a scaling exponent ($\beta = \mu/(2+\mu)$, equation (10)) and coefficient (K_D) are derived from at least five impact crater simulations using least squares fits.

Targets with larger f lead to a shift of scaling relationships to smaller dimensionless crater diameters (π_D) and thus smaller transient crater diameters (Figure 3a). This demonstrates that increasing the coefficient of friction reduces the crater efficiency as expected since f controls the material strength at pressure (section 4.1). We note that the reduced crater efficiency in targets with different coefficients of friction is substantial. For example, for L = 25–1000 m, transient crater diameters for a target with f = 0.8 (such as f for sands or rocks) are reduced by ~25–40% compared to a target with f = 0.1 (such as wet sand).

To examine the effect of porosity on crater sizes, we performed 30 additional simulations for materials with a constant coefficient of friction (f = 0.6) but with different porosities (Φ = 10, 20, 30, 40, and 50%, Figure 3b). The presence of porosity causes a reduction of crater efficiency through the compaction of pores, such that less energy is available for the crater excavation [e.g., *Zel'Dovich and Raizer*, 1966; *Love et al.*, 1993]. A change in porosity from Φ = 10 to Φ = 50% causes a decrease of about ~20–25% in π_D. Although the crater efficiency decreases with π_D, we emphasize that it does not necessarily imply a decrease in transient crater diameters with porosity because of the corresponding reduction in target density. Results are also compared to the dry sand scaling [*Holsapple and Housen*, 2007], and the scaling relationships for targets with f = 0.6–0.8 and Φ = 30–40% provide a good match as shown in section 4.2.

To develop robust scaling laws and find eventual relationships between scaling parameters and target properties, the parameter space spanned by the friction coefficient and porosity was extended to additional setups, where porosity Φ = 0, 1, 2, 3, 5, 6, 8, 9, 10, 12, 20, 30, 40, and 50% and f = 0.1, 0.2, 0.4, 0.6,

Table 3. Comparison of Parameters Resulting From This Study and Previous Experimental Results[a]

Material	Target Properties		Scaling Parameters	
	Friction	Porosity	K_d	β
Experimental results				
Water[b]	0.0	0%	1.880	−0.222
Water saturated sand[b]	~0.1	~0%	1.600	−0.220
Dense sand[c]	~0.7	30–40%	1.704	−0.167
Dense sand[d]	~0.7	30–40%	1.560	−0.170
Loose sand[e]	0.52	~40%	1.424	−0.175
This work				
Water analog	0.0	0%	1.735	−0.222
Wet-sand analog	0.1	0%	1.615	−0.218
Sand analog	0.6	30%	1.660	−0.169
Sand analog	0.6	40%	1.473	−0.175
Sand analog	0.8	30%	1.623	−0.164
Sand analog	0.8	40%	1.496	−0.166

[a]All scaling parameters are derived from transient crater diameters measured from the preimpact surface. Friction is indicated by coefficients of friction in iSALE.
[b]After *Schmidt and Housen* [1987] scaling laws for water and gravity scaling of wet sand.
[c]After *Schmidt* [1980].
[d]After *Holsapple and Housen* [2007, Table 1], often referred to as the dry sand scaling, here calculated with ρ = 1700 kg/m^3 and δ = 3000 kg/m^3 and multiplied by a constant factor of 1.3.
[e]After *Gault and Wedekind* [1977].

0.8, 0.9, and 1.0. About 600 numerical simulations have been performed, and the resulting scaling parameters for all possible combinations are summarized in Table 4. The dependencies of scaling parameters (μ and K_D) on target properties (f and Φ) are plotted in Figure 4 for selected combinations. The scaling exponent β is here converted to the more frequently used velocity-scaling exponent μ using equation (10).

In the first step, we describe the influence of target properties on the scaling exponent (μ). Results indicate that μ ranges from 0.56 (for a frictionless target), close to the energy scaling, to 0.39 (for target with $f \geq$ 0.6–0.8), close to the momentum scaling (Figure 4a). However, we note that both extreme values still remain clearly distinguishable from the energy and momentum scaling. The highest μ (0.44–0.56) are computed for nonporous cases since less of the energy deposited in a nonporous target is dissipated during the formation of the crater [*Pierazzo*, 1997]. Depending on the target's porosity, μ is shifted toward higher or lower values, which indicates that porosity also influences the resulting μ. A better description of this effect is depicted in Figure 4c, where μ is plotted as a function of Φ. Surprisingly, materials with large porosity, i.e.,

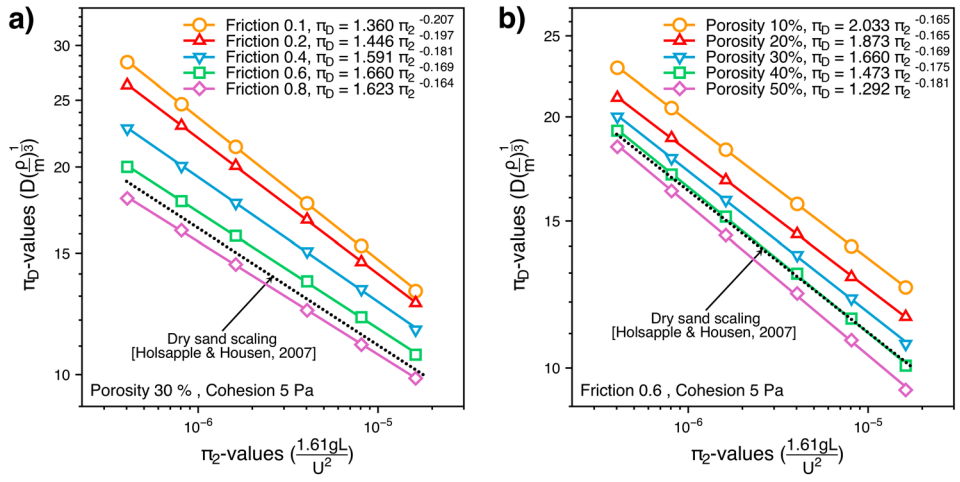

Figure 3. Dimensionless crater diameters (π_D) plotted versus the gravity-scaled values (π_2) (log-log plot) for granular targets (cohesion Y_0 = 5 Pa) with (a) porosity Φ = 30% and varying coefficient of frictions (0.1 $\leq f \leq$ 0.8) and (b) with f = 0.6 and 10% $\leq \Phi \leq$ 50%. Power laws are fitted through data points using a least squares method. The dry sand scaling [*Holsapple and Housen*, 2007] is plotted for reference.

Table 4. Scaling Relationships for the Range of Coefficient of Friction and of Porosity Listed in Table 1 Written in the Form $\pi_D = K_D\,\pi_2^{-\beta a}$

Friction/Porosity	0 %	1 %	2 %	3 %	5 %	6 %	8 %
0.0	$1.735\,\pi_2^{-0.222}$	-	-	-	-	-	-
0.1	$1.615\,\pi_2^{-0.218}$	$1.767\,\pi_2^{-0.208}$	$1.836\,\pi_2^{-0.203}$	$1.772\,\pi_2^{-0.205}$	$1.778\,\pi_2^{-0.202}$	$1.715\,\pi_2^{-0.204}$	$1.689\,\pi_2^{-0.203}$
0.2	$1.711\,\pi_2^{-0.208}$	$1.859\,\pi_2^{-0.199}$	$1.943\,\pi_2^{-0.193}$	$1.901\,\pi_2^{-0.193}$	$1.875\,\pi_2^{-0.192}$	$1.791\,\pi_2^{-0.195}$	$1.770\,\pi_2^{-0.194}$
0.4	$1.754\,\pi_2^{-0.195}$	$2.025\,\pi_2^{-0.182}$	$2.058\,\pi_2^{-0.179}$	$2.102\,\pi_2^{-0.176}$	$2.096\,\pi_2^{-0.175}$	$2.021\,\pi_2^{-0.177}$	$1.992\,\pi_2^{-0.176}$
0.6	$1.902\,\pi_2^{-0.181}$	$2.093\,\pi_2^{-0.171}$	$2.073\,\pi_2^{-0.171}$	$2.108\,\pi_2^{-0.169}$	$2.225\,\pi_2^{-0.162}$	$2.125\,\pi_2^{-0.165}$	$2.040\,\pi_2^{-0.166}$
0.8	$1.842\,\pi_2^{-0.181}$	$2.043\,\pi_2^{-0.166}$	$2.063\,\pi_2^{-0.165}$	$2.066\,\pi_2^{-0.164}$	$2.100\,\pi_2^{-0.160}$	$2.115\,\pi_2^{-0.158}$	$2.048\,\pi_2^{-0.159}$
0.9	$1.741\,\pi_2^{-0.187}$	$1.990\,\pi_2^{-0.166}$	$1.949\,\pi_2^{-0.168}$	$1.861\,\pi_2^{-0.171}$	$2.011\,\pi_2^{-0.162}$	$1.922\,\pi_2^{-0.165}$	$1.932\,\pi_2^{-0.162}$
1.0	-	-	-	-	-	-	-
Friction/Porosity	9 %	10 %	12 %	20 %	30 %	40 %	50 %
0.0	-	-	-	-	-	-	-
0.1	$1.639\,\pi_2^{-0.204}$	$1.730\,\pi_2^{-0.199}$	$1.585\,\pi_2^{-0.205}$	$1.513\,\pi_2^{-0.203}$	$1.360\,\pi_2^{-0.207}$	$1.197\,\pi_2^{-0.212}$	$0.995\,\pi_2^{-0.222}$
0.2	$1.738\,\pi_2^{-0.195}$	$1.809\,\pi_2^{-0.190}$	$1.689\,\pi_2^{-0.195}$	$1.618\,\pi_2^{-0.193}$	$1.446\,\pi_2^{-0.197}$	$1.293\,\pi_2^{-0.201}$	$1.092\,\pi_2^{-0.210}$
0.4	$1.949\,\pi_2^{-0.177}$	$1.999\,\pi_2^{-0.174}$	$1.862\,\pi_2^{-0.178}$	$1.746\,\pi_2^{-0.178}$	$1.591\,\pi_2^{-0.181}$	$1.420\,\pi_2^{-0.186}$	$1.225\,\pi_2^{-0.193}$
0.6	$2.038\,\pi_2^{-0.165}$	$2.033\,\pi_2^{-0.165}$	$1.984\,\pi_2^{-0.165}$	$1.873\,\pi_2^{-0.165}$	$1.660\,\pi_2^{-0.169}$	$1.473\,\pi_2^{-0.175}$	$1.292\,\pi_2^{-0.181}$
0.8	$2.004\,\pi_2^{-0.160}$	$1.994\,\pi_2^{-0.159}$	$1.991\,\pi_2^{-0.158}$	$1.840\,\pi_2^{-0.159}$	$1.623\,\pi_2^{-0.164}$	$1.496\,\pi_2^{-0.166}$	$1.277\,\pi_2^{-0.175}$
0.9	$1.768\,\pi_2^{-0.169}$	$1.972\,\pi_2^{-0.158}$	$1.699\,\pi_2^{-0.169}$	$1.635\,\pi_2^{-0.166}$	$1.584\,\pi_2^{-0.164}$	$1.397\,\pi_2^{-0.170}$	$1.210\,\pi_2^{-0.177}$
1.0	-	$1.884\,\pi_2^{-0.162}$	-	$1.872\,\pi_2^{-0.155}$	$1.422\,\pi_2^{-0.172}$	$1.353\,\pi_2^{-0.173}$	$1.530\,\pi_2^{-0.160}$

[a]Scaling exponents β can be converted into the velocity-scaling exponent μ using $\mu = (2\beta)/(1-\beta)$.

materials with significant dissipation of energy, also feature large μ. The effect of porosity on μ seems thus to be separated into two regimes. For $\Phi < \sim$10%, the rapid decay of μ appears to be independent of the target's coefficient of friction. In the second regime ($\Phi \geq 10\%$), a slight linear increase of μ with Φ is observed. This particular detail is not yet fully understood and requires further attention. However, we point out that the coefficient of friction has, in general, a much stronger influence on μ than porosity.

In terms of the scaling coefficient (K_D), however, the target porosity clearly has a stronger effect than the friction coefficient (Figures 4b and 4d). K_D generally decreases linearly with porosity, but for $\Phi < \sim$5% the results deviate from the linear relationship and converge toward smaller K_D for nonporous targets. This behavior at small porosities is difficult to explain but is consistent with our findings for the scaling exponents above (Figure 4c). In addition, we find that scaling coefficients increase with increasing coefficient of friction for $f \leq 0.6$ but decrease for $f > 0.6$ (Figure 4b). In general, K_D values are constant within ±5% over the whole range of studied coefficients of friction, while K_D decreases by about 25–30% if target porosity increases from Φ = 10% to 30%.

To further investigate the robustness of these findings, we compared our results to previous numerical experiments that employed a similar setup but with lower impact velocity (U = 5 km/s) and a quartzite equation of state [*Wünnemann et al*., 2011]. If these crater relationships are recalculated to include only simple craters, results exhibit comparable trends in the above described relationships (Figure 4). However, we underline that if scaling parameters are plugged into equation (10), our π_D values are up to 10% higher than those in *Wünnemann et al*. [2011]. This may indicate a possible additional velocity dependence, which is not accounted for through π_2 (section 3).

5.2. Dependencies of the Scaling Results on Strength and Porosity Model Parameters

To provide a measure of the uncertainty induced by assuming a constant limiting strength at high pressure Y_{LIM} and constant compaction parameters, a sensitivity analysis has been conducted (Figure 5, model parameters are summarized in Table 5). To assess the influence of Y_{LIM} on the obtained results, we derived scaling parameters for targets with f = 0.6, Φ = 20%, and cohesion of 5 Pa for a range of Y_{LIM}. The results show that the effect of the strength limit is minor, with only a small decrease (~5%) of the scaling exponents for a very low Y_{LIM} = 0.1 GPa (Figure 5a). For $Y_{\mathrm{LIM}} > 0.5$ GPa, the scaling exponent is not affected at all consistent with *Güldemeister et al*. [2015].

We investigate the effect of the choice of compaction parameters K and α_x, using a range of values similar to that in *Collins et al*. [2011] and *Davison et al*. [2016]. Our results indicate a minor and probably

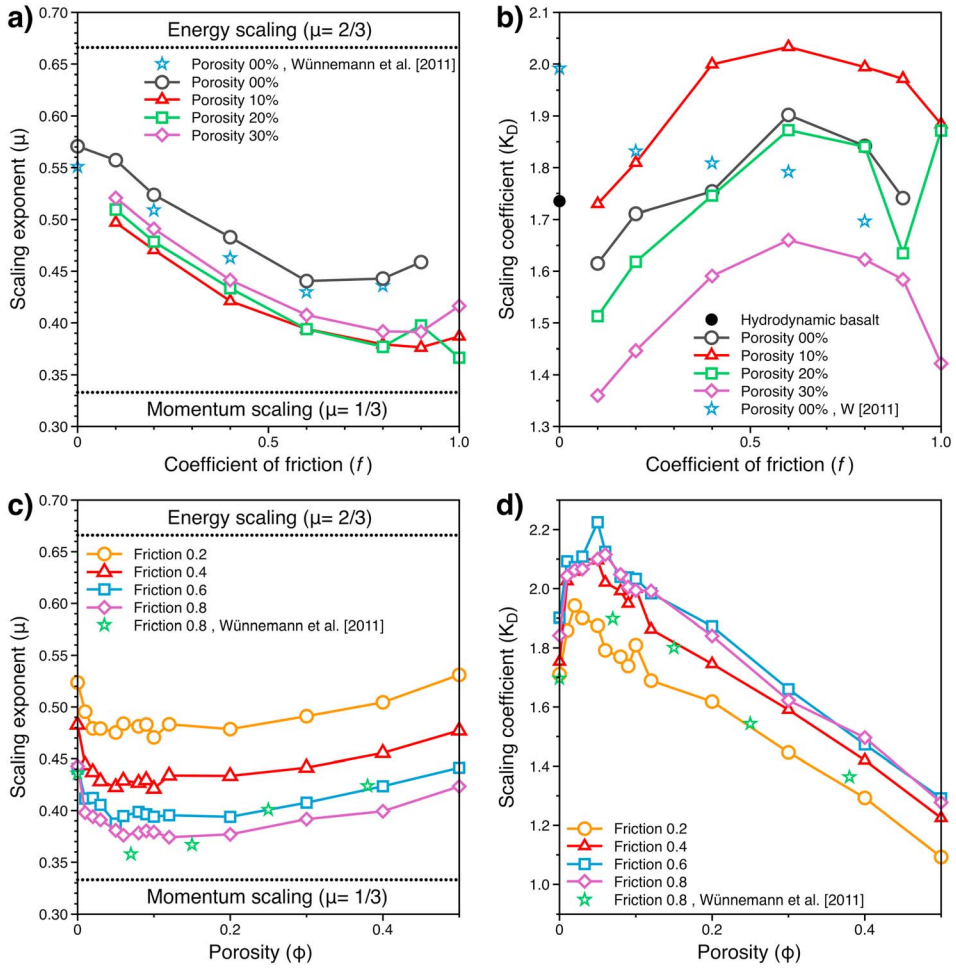

Figure 4. Crater scaling exponent (μ) and coefficient (K_D) as a function of (a, b) target friction coefficient f and (c, d) porosity Φ, derived from at least five simulations using different L (25 m $\leq L \leq$ 1000 m). Empty stars depict recapitulated data for simple craters from *Wünnemann et al.* [2011].

negligible influence on the transient crater diameter (Figures 5b and 5c). In contrast, the onset of plastic compaction (ε_e), which can be considered as the critical strain below which compaction is irreversible and describes the stress that is needed to permanently crush the material [*Wünnemann et al.*, 2006; *Collins et al.*, 2011; *Güldemeister et al.*, 2013; *Luther et al.*, 2017], and the bulk sound speed ratio (χ) of porous material and the nonporous matrix are the most influential parameters (Figure 5d). Two cases were investigated.

First, the onset of plastic compaction was chosen to be $\varepsilon_e = -0.01$ (i.e., the onset of plastic compaction starts when a given volume is compressed to 99% of its initial volume), which represents well the behavior observed for terrestrial dry porous sandstones with Φ = 15–20% [*Wong and Baud*, 1999; *Vajdova et al.*, 2004]. As porosity decreases in a rock, the critical pressure (i.e., the pressure needed to start compaction in a sample) and, thus, the corresponding volumetric strain required for the onset of compaction also increases [*Wong and Baud*, 1999]. A compilation of critical pressures for carbonate rocks with different porosities indicates the critical pressure to be relatively constant for $\Phi \geq 15\%$ [*Vajdova et al.*, 2004]. However, for rocks with $\Phi < 15\%$, the critical pressure to start compaction increases with decreasing porosity, with a critical pressure about 10 times larger for Φ = 3% than for Φ = 15% [*Vajdova et al.*, 2004].

In the second case, we thus assume the threshold value for compaction to be 10 times larger (in terms of the absolute value) than in the first case ($\varepsilon_e = -0.1$). In both cases, the initial porosity was held constant in order to

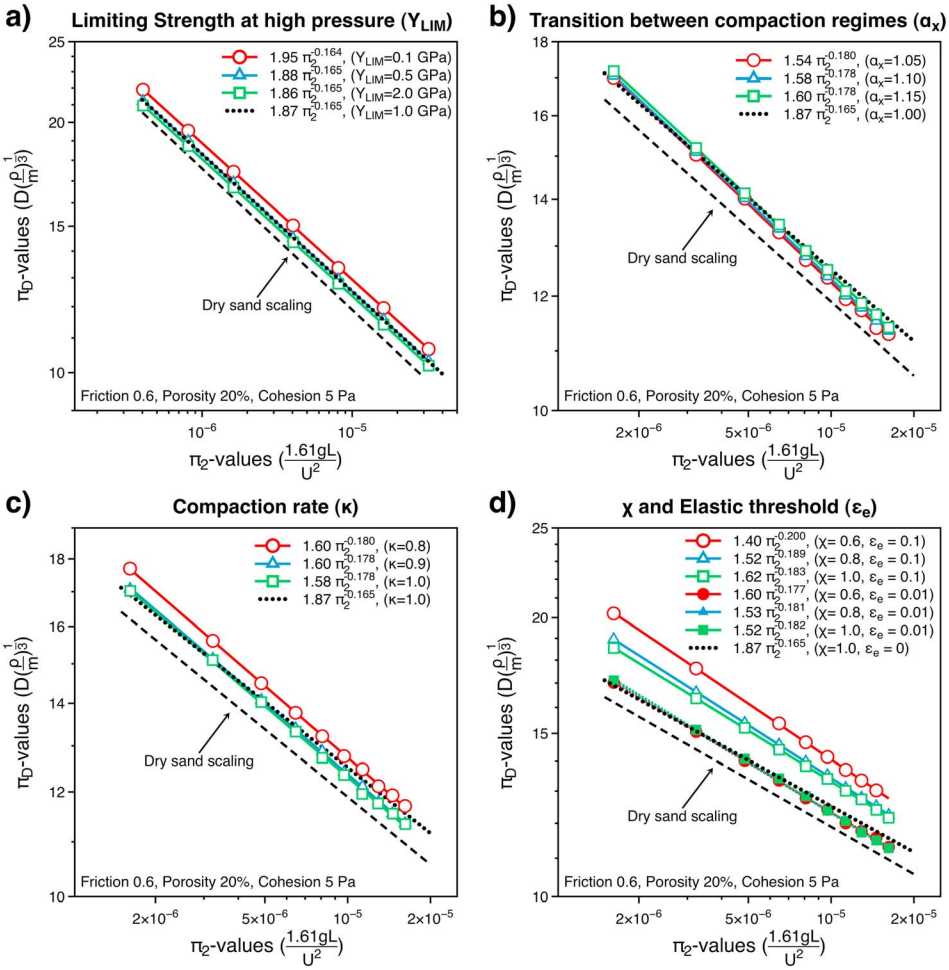

Figure 5. Scaling relationships for (a) different limiting strengths at high pressure Y_{LIM} and (b–d) for various porosity model parameters using projectiles diameters $100 \leq L \leq 1000$ m, an impact speed of $U = 12.7$ km/s, and a gravity $g = 1.62$ m/s^2. The black dotted line depicts the case where porosity model parameters are held constant. Table 5 summarizes strength and porosity model parameters for each case. The experimental dry sand scaling ($f \sim 0.7$, $\Phi = 30$–40%) is shown for comparison [*Holsapple and Housen*, 2007].

compare results and bulk sound speed ratios were varied over a plausible range ($\chi = 0.6$–1.0). Both results are compared to the case in which the elastic compaction regime is neglected ($\varepsilon_e = 0$, Figure 5, black dotted line), which is a good approximation for low-strength, high-porosity targets, such as sand [e.g., *Miljković et al.*, 2012]. The difference between the two cases with $\varepsilon_e = -0.01$ and $\chi = 0.6$ or $\chi = 1.0$, respectively, is only about ±2%. With $\varepsilon_e = -0.1$, more significant deviations from the model with $\varepsilon_e = -0.01$ are obtained, with an ~5–20% increase in crater efficiency depending on the bulk sound speed ratio χ. However, as porosity decreases, χ gets closer to 1. Thus, we expect the crater efficiency more to be ~5–10% larger for low-porosity target. This simple test indicates that the two compaction model parameters ε_e and χ likely depend on the initial porosity of the material. For the current work in which ε_e and χ have not been adjusted for low porosities, the results obtained for very small porosity have thus to be interpreted with caution.

5.3. The Effect of Cohesion, Coefficient of Friction, and Porosity on Transient Crater Diameter for Strength and Gravity-Dominated Craters

So far, we have focused on the gravity regime only, i.e., granular targets with negligible cohesion Y_0. In this section, we further investigate how (a) cohesion, (b) friction coefficient, and (c) porosity affect transient crater diameters across the strength-gravity regime transition (Figure 6). For competent targets (such as material

Table 5. Summary of Strength and Model Porosity Parameters Investigated in Figure 5

Figure	Porosity (%)	ε_e (%)	χ	α_X	κ	Y_{LIM} (GPa)
a	20	0%	1.0	1.00	0.98	0.1
a	20	0%	1.0	1.00	0.98	0.5
a	20	0%	1.0	1.00	0.98	2.0
b	20	−1%	0.6	1.05	0.98	1.0
b	20	−1%	0.6	1.10	0.98	1.0
b	20	−1%	0.6	1.15	0.98	1.0
c	20	−1%	0.6	1.10	0.80	1.0
c	20	−1%	0.6	1.10	0.90	1.0
c	20	−1%	0.6	1.10	1.00	1.0
d	20	−10%	0.6	1.10	0.98	1.0
d	20	−10%	0.8	1.10	0.98	1.0
d	20	−10%	1.0	1.10	0.98	1.0
d	20	−1%	0.6	1.10	0.98	1.0
d	20	−1%	0.8	1.10	0.98	1.0
d	20	−1%	1.0	1.10	0.98	1.0
In main study	20	0%	1.0	1.00	0.98	1.0

M2; Figure 1) the effect of strength (represented by the term π_3) on scaling is no longer negligible. Both the strength and gravity regime are considered in the universally applicable but more complex form of the scaling laws (equation (8)) and used to fit results from numerical or laboratory experiments. In addition to the scaling coefficient and exponent, an effective strength parameter, Y_{EFF}, has to be taken into consideration. If we still assume the strength of the target to have only a small influence on the compaction parameters (section 5.2), the scaling parameter μ and ν should be the same in the strength and the gravity regime (equations (9) and (10)). Therefore, materials with the same coefficient of friction and porosity should have the same scaling parameters, independent of their effective strength. As a consequence, the previously derived scaling parameters (section 5.1) for granular targets should be applicable for cohesive targets with the same coefficient of friction and porosity. Y_{EFF} is therefore the only remaining unknown parameter. We derive Y_{EFF} by fitting equation (8) to the model data (π_D for a given π_2; Figure 6) using a least squares method.

We find that with increasing cohesion π_D decreases due to the stronger resistance of the target to the opening of the crater cavity (Figure 6a). Although the transition from the strength to the gravity regime is gradual, it can clearly be seen that the transition occurs at larger π_2 values when Y_0 is larger. We emphasize that this transition is also affected by other target properties such as the coefficient of friction and porosity. In both cases (Figures 6b and 6c), the strength-gravity transition is shifted toward larger π_2 and smaller π_D due to decreasing crater efficiency with increasing coefficient of friction and porosity.

For comparison, a scaling for wet sand based on cratering experiments [*Schmidt and Housen*, 1987] is given because of its supposedly good approximation of the pure gravity regime for competent rocks with no or very little porosity [*Holsapple and Housen*, 2017]. However, some of our model results do not support this assumption as they clearly deviate from wet-sand scaling. Only targets with low coefficient of friction and porosity do seem to approach the wet-sand scaling (Figures 6b and 6c). We compared these results with numerical experiments for competent rocks, quartzite, and sandstones targets, which are calibrated against laboratory-scale data [*Poelchau et al*., 2013; *Güldemeister et al*., 2015]. The main differences between *Güldemeister et al*. [2015] and our model setup are that their crater relationships are derived over a larger range of projectile diameters (0.012–500 000 m), at Earth gravity (g = 9.81), for smaller velocity (U = 5 km/s), and with an equation of state for quartzite [*Melosh*, 2007]. Moreover, the strength of the target is described by a more sophisticated strength model [*Collins et al*., 2004] in which both the strength properties of the damaged (damaged coefficient of friction f_{dam} = 0.67 and damaged cohesion Y_{dam} = 0) and intact material are different (intact coefficient of friction f_{int} = 0.8 and intact cohesion Y_{int} = 96.9 and 22.75 MPa for quartzite and sandstone targets, respectively). Because these strength model parameters are calibrated against laboratory-scale data, i.e., against targets which are expected to have a much larger cohesion than materials at planetary scale, their numerical data indicate much smaller transient crater diameters. However, regardless of the strength model used, the scaling parameters we found in our study for granular targets should be the same for sandstone and quartzite targets with the same porosity and coefficient of friction (ranging from f_{dam} to f_{int}).

The scaling exponents reported by *Güldemeister et al*. [2015] (derived from transient crater diameters in the gravity regime) are much closer to the wet-sand scaling exponent μ = 0.55, with μ for quartzite (μ = 0.49)

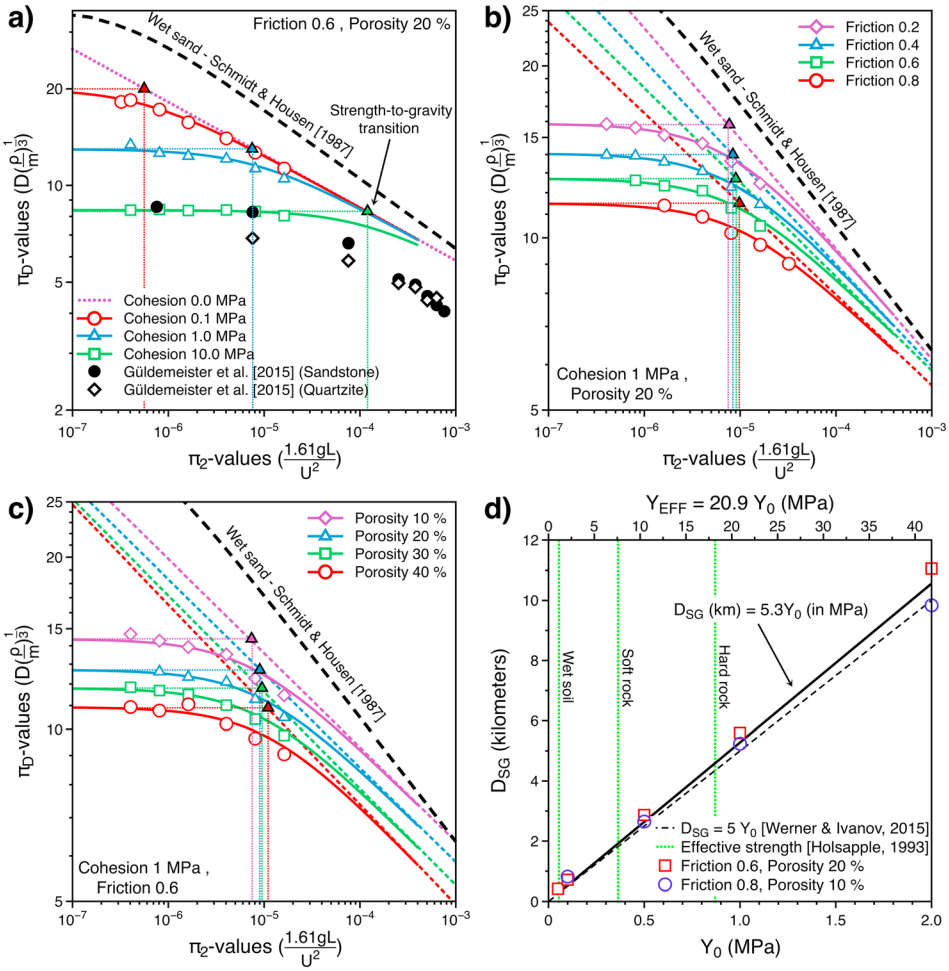

Figure 6. (a) Dimensionless crater diameter (π_D) versus the gravity-scaled size (π_2) for targets with (a) $f = 0.6$, $\Phi = 20\%$, and varying cohesions $Y_0 = 0.1$, 1, 10 MPa; (b) $\Phi = 20\%$, $Y_0 = 1$ MPa, and varying $f = 0.2$–0.8; (c) $f = 0.6$, $Y_0 = 1$ MPa, and varying $\Phi = 10$–40%. The strength-to-gravity regime transition is indicated for each combination of target properties by colored triangles and dotted lines. Note that the limited amount of data in the gravity regime (large π_2) is due to our limitation to simple craters and targets with relatively large cohesion. (d) Strength-to-gravity transition diameter (D_{SG}) versus the cohesion in iSALE (Y_0, lower x axis) and the effective strength (Y_{EFF}, upper x axis) for targets with $f = 0.6$, 0.8, $\Phi = 20$, 10%, and varying cohesions Y_0. Note that the relation from *Werner and Ivanov* [2015] is derived from numerical experiments conducted in *Wünnemann et al.* [2011] for a nonporous target with $f = 0.8$ and varying cohesions.

and sandstone ($\mu = 0.55$) than our data for similar target properties (quartzite: $\mu \sim 0.44$ for $\Phi = 0\%$ and $f = 0.6$–0.8, sandstone: $\mu \sim 0.39$–0.41 for $\Phi = 30\%$ and $f = 0.6$–0.8). The largest difference is observed for the sandstone case, for the porous target ($\Phi = 30\%$). We argue that the possibly large ε_e value (-0.1) for the sandstone target in *Güldemeister et al.* [2015] is probably the reason for the large discrepancy in μ, as shown in Figure 5d.

Relations in Figure 6d are plotted to give the reader the possibility to relate the effective strength in crater scaling relationships to the cohesion in our numerical models and to the strength-to-gravity transition crater diameter. In both cases, we find the relation between the effective strength and the cohesion Y_0 in the Drucker-Prager strength model to be well approximated by

$$Y_{\mathrm{EFF}} = 20.9\, Y_0, \tag{11}$$

and the relation between Y_0 and D_{SG} by

$$D_{\mathrm{SG}}(\mathrm{km}) \cong 5.3\, Y_0\ (\mathrm{MPa}). \tag{12}$$

Note that both equations are dependent on target properties but are here found to be approximately the same for $f = 0.6$–0.8 and $\Phi = 0$–20%.

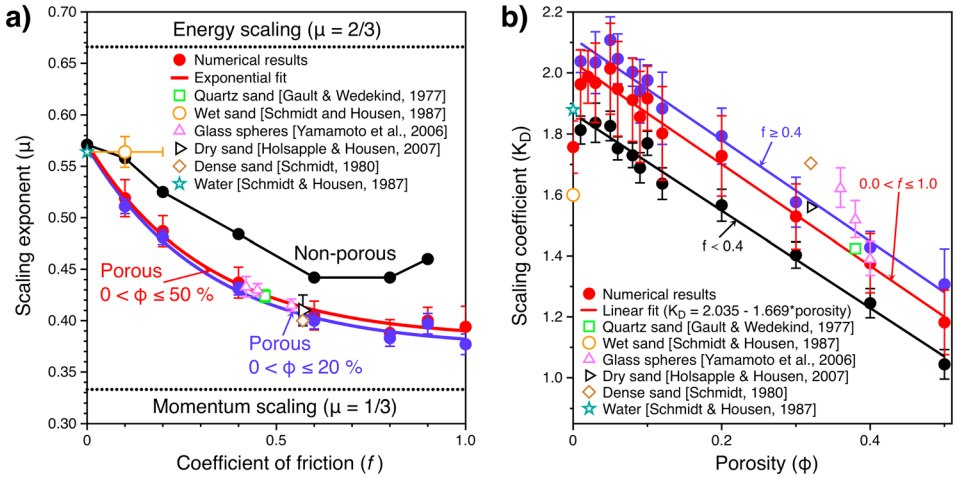

Figure 7. (a) Scaling exponents (μ) as a function of the coefficient of friction ($0 \le f \le 1.0$) for targets with $0 < \Phi \le 20\%$ (blue, equation (13)), for targets with $0 < \Phi \le 50\%$ (red, equation (14)), and for nonporous targets (black). (b) Scaling coefficients (K_D) as a function of porosity for targets with $0 < \Phi \le 50\%$ and $f \ge 0.4$ (blue, equation (15)), $f < 0.4$ (black, equation (16)), and $0 \le f \le 1.0$ (red, equation (17)). For our numerical results, dots represent the mean values and error bars depict one standard deviation. Additional experimental studies are plotted for comparison with their uncertainties, if available.

6. Incorporating the Effects of Coefficient of Friction and Porosity in the π Group Scaling Law

The coefficient of friction (f) and porosity (Φ) can be incorporated in the π group scaling law by expressing the scaling parameters (μ, K_D) as a function of f and Φ (Figure 4). We now make an attempt to generalize this approach. Our results suggest that μ is mostly influenced by the coefficient of friction (Figure 4a) and K_D mostly by the porosity of the target (Figure 4d). One approach to generalize the previous parameterizations may thus be to assume that (1) μ is independent of target porosity and (2) K_D is independent of the friction coefficient. Assumption (1) is relatively well satisfied for porous materials with $0 < \Phi \le 20\%$, where only a minor change with increasing porosity is observed (Figure 4c). This simplification is also in good agreement with previous numerical [*Wünnemann et al.*, 2011] and experimental studies [*Housen and Holsapple*, 2011] in which μ was found to vary only slightly with porosity. Assumption (2) may be less well satisfied; the scaling coefficients vary by ±15% using constant coefficient of friction but varying porosity. However, for targets with $f \ge 0.4$, errors introduced by assumption (2) are smaller (Figure 4b and Table 4). Figures 4b and 4c yield only a single value for K_D and μ for fixed porosity and fixed coefficient of friction, respectively. Therefore, generalized relationships for the variation of scaling law parameters as a function of friction coefficient and porosity can be obtained (Figure 7).

We find a decay of μ with increasing coefficient of friction (Figure 7a) that can be approximated by an exponential relationship:

$$\mu = 0.374 + 0.012\exp(-3.175(f - 0.884)), \quad \text{for} \quad 0 < \Phi \le 20\%, \tag{13}$$

$$\mu = 0.383 + 0.004\exp(-3.031(f - 1.278)), \quad \text{for} \quad 0 < \Phi \le 50\%. \tag{14}$$

To account for the entire range of friction coefficient, including the hydrodynamic case ($f = 0$), only an (empirical) exponential fit can match the numerically obtained results satisfactorily. Note that equations (13) and (14) are applicable only for porous targets. The relationships derived for nonporous targets clearly deviate from the porous cases (see discussion in section 7.2).

In contrast, the relationship between the scaling coefficients (K_D) and porosity (Φ) is best described by a linear dependence of K_D on Φ (Figure 7b) that can be fit by the following expressions:

$$K_D = 2.114 - 1.667\Phi, \quad f \ge 0.4, \qquad 0 < \Phi \le 50\%. \tag{15}$$

$$K_D = 1.867 - 1.596\Phi, f < 0.4, \qquad 0 < \Phi \le 50\%. \tag{16}$$

$$K_D = 2.035 - 1.669\Phi, \quad 0 < f < 1.0, \quad 0 < \Phi \le 50\%. \tag{17}$$

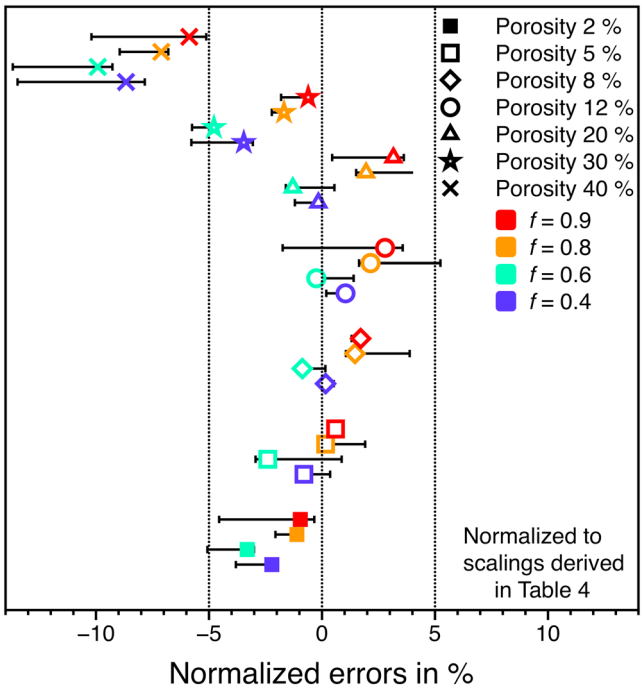

Figure 8. Scaling relationships derived from equations (13) and (15) normalized to scaling results given in Table 4 (i.e., scaling relationships derived from the least squares method, with no assumptions). Scaling relationships are applied over a projectile diameter range of $25 \leq L \leq 1000$ m. The average values are represented by colored symbols, the minimum-maximum range is denoted by the error bars.

To test the validity of our assumptions (1) and (2), we compare our empirical fits to experimental studies in which scaling parameters have been derived from craters solely forming in the gravity regime in various types of material (Figure 7). The experiments mostly cover two end-members: one with strengthless and low friction coefficient and porosity materials (water and wet sand with $\Phi \sim 0\%$ and $f \leq 0.1$) and one of porous materials with $\Phi \sim 30$–40% and $f \sim 0.4$–0.7 (dry sand, dense sand, and glass spheres). The uncertainty in the scaling exponent for the dry sand scaling is not reported in *Holsapple and Housen* [2007], while the wet-sand gravity scaling [*Schmidt and Housen*, 1987] is estimated from water and dry sand scaling because only few data fell into the gravity regime [*Holsapple and Housen*, 2017]. Uncertainties are therefore not shown in both cases. Note that the transient crater diameter for targets composed of glass microsphere [*Yamamoto et al.*, 2006] is defined as the rim-to-rim diameter at the onset of crater collapse. For comparison with other data, we thus divided their data by 1.25 to account (to first order) for the difference between transient and final rim-to-rim crater diameters [*Grieve and Garvin*, 1984; *Collins et al.*, 2005]. An uncertainty of ±5% is assumed here to account for a possible influence of target properties on crater collapse.

We find that the exponential relations (13) and (14) are in good agreement with experimental data for porous materials. Also, the empirical parameterization for nonporous material fits the data well for water and wet sand. Assumption (1) seems thus adequate over the range of projectiles studied here. Assumption (2) also leads to good agreement between numerical results and experimental data (Figure 7b), which is well indicated by the clustering of most of the sand and glass sphere targets ($f \approx 0.4$–0.7) along equation (15). K_D, however, appears to be not fully independent of the coefficient of friction (equations (15)–(17)). Nevertheless, the fit lies well within the uncertainty range of 1 standard deviation of our numerical results.

After testing the feasibility of our approximations, we now investigate their ability to approximate actual scaling parameters. We use equations (13) and (15) to estimate scaling parameters for a range of target properties and compare them to our actual obtained numerical simulation results (Table 4). Figure 8 shows that the derived relations (13) and (14) provide a reasonable approximation to the inferred scaling relationships for porosities $\leq$30% and coefficients of friction $\geq$0.4. The misfit between our empirical relations and our numerical experiments is less than ±5%. Note that equations (14) and (15) perform equally well and thus provide equally good approximations but are not explicitly shown.

7. Discussion

7.1. Model Limitations and Applicability to Crater Scaling Relationships

As mentioned in section 4, our approach is simplified and subject to future improvements, mostly concerning the employed strength and compaction models. The biggest simplifications are that (1) the compaction model parameters are held constant for all initial porosities, regardless of the strength of the target, and

that (2) the elastic compaction regime in the target is neglected, which omits any crushing strength the material may have. As porosity in a rock decreases, however, grains become more tightly interlocked and a low-porosity target should thus be much harder to compact than a highly porous target, such as lunar regolith [*Slyuta*, 2014]. Based on the critical pressure (and strain) for the onset of plastic compaction in carbonate rocks on Earth and a sensitivity analysis of compaction model parameters, we estimated that crater scaling relationships for targets with $\Phi < 10$–15% could be significantly influenced by our simplification (up to 20% difference in cratering efficiency with respect to the constant case). However, we note that the critical pressure of carbonate rocks [e.g., *Wong and Baud*, 1999; *Vajdova et al*., 2004, and references therein] is usually measured at laboratory scale, and it is essentially unknown how this can be transferred to planetary scale and whether the increase in critical pressure (see section 5.2) is comparable at small and large scales, where widespread fractures and joints may exist.

Furthermore, we used the Drucker-Prager strength model to describe the behavior of granular materials, cohesive soils, and rocks. The crater scaling results summarized in Table 4 and the approximation made in section 6 therefore need to be interpreted with caution for $\Phi < 10$–15%, a range that may, e.g., be relevant for basaltic lunar mare [*Kiefer et al*., 2012]. Over this range of porosity, crater scalings may be closer to the scaling for nonporous targets (Figure 7a). Since fracturing is also neglected in our numerical approach, equations (11)–(17) and Table 4 may be strictly valid only for weak and low-strength materials. If we assume the effective strength value for soft rocks derived from *Holsapple* [1993] to be an adequate upper limit (Figure 6d), equations (11)–(17) might be inappropriate for effective strengths $Y_{EFF} > 7.5$ MPa (which corresponds to $Y_0 = 350$ kPa using equation (11)).

7.2. Effects of Target Properties on Crater Scaling Laws

We have studied the importance of target properties (coefficient of friction, porosity, and cohesion) on the size of a simple crater whose growth is dominated by either strength or gravity. In general, our results in the gravity regime (i.e., at large π_2 for rock-like materials or across the entire π_2 range for granular targets) show that both the coefficient of friction and porosity influence the transient crater size observed during impact crater formation. However, we emphasize that friction coefficient and porosity have different effects on crater growth, which is illustrated by different scaling relationships (Figure 4).

Previously, experimental studies showed that porous materials have scaling exponents that are close to the momentum scaling ($\mu = 0.37$–0.40) [*Holsapple and Schmidt*, 1987, and references therein] and smaller than for nonporous materials ($\mu = 0.55$–0.60), even though the exact reason for this behavior remains uncertain [*Holsapple and Schmidt*, 1987; *Housen and Holsapple*, 2011]. Our results indicate that the relatively small range of μ for experimentally studied porous materials is probably caused by the relatively similar friction coefficients of such materials: sand [e.g., *Schmidt*, 1980; *Schmidt and Housen*, 1987]; mixture of sand, perlite, fly ash and water [e.g., *Housen and Holsapple*, 2003]; and glass beads [*Yamamoto et al*., 2006]. Our data support this explanation (Figures 4a and 7a and Table 4) since for a large number of porous materials (with $0.6 \leq f \leq 0.9$) we observed scaling exponents in the range $0.37 \leq \mu \leq 0.40$. Scaling exponents for porous materials are therefore closer to the momentum scaling due to the effect of the coefficient of friction.

In contrast, porosity has only a minor effect on whether crater relationships scale with the energy or the momentum of the impactor. This result is consistent with recent numerical [*Wünnemann et al*., 2011; *Güldemeister et al*., 2015] and experimental studies [e.g., *Housen and Holsapple*, 2003; *Housen and Holsapple*, 2011]. The decrease in crater efficiency with increasing porosity is mainly reflected by the scaling coefficient K_D for which a linear decrease is observed with increasing porosity (Figure 7b), consistent with *Wünnemann et al*. [2011]. However, both higher friction coefficient and porosity enhance dissipation in a material and should therefore lead to smaller scaling exponents μ [*Holsapple and Schmidt*, 1987]. The exact mechanism linking the porosity-induced reduction in crater efficiency to a decrease in K_D and the friction coefficient-induced decrease to changes in μ remains unknown. One reason could be related to differences in transient crater morphology (see supporting information Text S3), which depends on impactor and target properties and on the selected transient crater definition (see supporting information Text S1). For targets with $0 < \Phi \leq 30\%$, we find indeed that the depth-diameter ratios (*d/D)* remain relatively constant for the same projectile diameter *L*. On the other hand, *d/D* increases considerably for larger porosity, possibly due to a deeper penetration depth as previously shown in impact experiments in low-density targets [*Kadono*, 1999; *Kadono and Fujiwara*, 2005].

For $\Phi > 30\%$, *d/D* increases, which in turn leads to a slight increase of μ for highly porous targets (Figure 4c). Possibly, this behavior would not be observed if the transient crater was defined based on a constant depth-diameter ratio. Moreover, we note that *d/D* is approximately constant for nonporous targets and the behavior of nonporous and porous targets differs significantly as reflected in the derived scaling parameters (Figures 4a–4d and 7a). In general, nonporous materials feature larger scaling exponents and a wider range ($0.44 \leq \mu \leq 0.56$, Table 4) than proposed by *Holsapple and Schmidt* [1987] ($0.55 \leq \mu \leq 0.60$). The reason for this discrepancy could be that no impact or large explosion experiments have been conducted in the gravity regime for nonporous materials except water [*Holsapple and Housen*, 2017] and that craters forming in rocks are generally assumed to scale in the same way as those in wet sand in the gravity regime [*Holsapple*, 1993].

7.3. The Effective Strength in Crater Scaling Laws

The strength term in scaling laws is often defined as an effective strength describing the target strength during the course of crater formation [*Holsapple*, 1993]. Since it may be an oversimplification to account for the complex material response on deformation only by a single scalar parameter, there is no consensus on which strength measure represents the target strength in the cratering process best [e.g., *Holsapple*, 1993; *Poelchau et al*., 2013; *Güldemeister et al*., 2015].

For targets such as the lunar regolith, the effective strength has been defined as the shear strength at failure [*Holsapple and Housen*, 2007]. For stronger materials such as rocks, however, the effective strength is derived from a combination of data from large chemical and nuclear explosion experiments for craters on the 10–100 m diameter range [*Schmidt et al*., 1986]. These cratering studies in rocks have been conducted in various geologies and have been grouped into generic materials [*Schmidt et al*., 1986]: soft rocks (such as sandstone, shale, weathered granite, and tuff) and hard rocks (such as basalt, granite, and tonalite) [Cooper, 1977]. The effective strength was found to be about ~1–10 MPa depending on target properties [*Holsapple*, 1993, Table 1; *Holsapple and Housen*, 2017, Table 5]. This range is in agreement with values reported in *Melosh* [1989, pp.116 and 120], where Y_{EFF} is ~1–2 MPa based on experiments on the strength-gravity transition in basalt targets. This implies a transition from the strength to the gravity regime at about 200–400 m on the lunar mare.

However, we point out several important limitations with the existing crater scaling laws for materials with cohesion (i.e., wet sand, soft rock, and hard rock scaling). Previous studies indicate that target properties vary substantially across a planetary surface at regional and global scale and also in between different bodies [*Cintala et al*., 1977; *Wood and Anderson*, 1978; *Pike*, 1980; *Kiefer et al*., 2012; *Robbins and Hynek*, 2012; *Wieczorek et al*., 2013]. Hence, although the effective strength of soft and hard rocks was derived for appropriate terrestrial materials, they may differ for other planetary bodies. Furthermore, there is a limited number of scaling relationships derived for various target properties.

As mentioned earlier, only a single crater relationship is available for rock-like materials and another one for dry sand and weak cohesive soils [*Holsapple and Housen*, 2007]. Differences in target properties are commonly characterized only by differences in effective strength and by the density contrast between the projectile and the target, whereas all other scaling parameters are held constant [e.g., *Holsapple*, 1993; *Richardson*, 2009; *Dundas et al*., 2010; *Marchi et al*., 2011]. Thus, the application of the two known relationships to targets with other properties may be complicated. As an example, *Dundas et al*. [2010] investigated the effects of target properties on crater statistics on an area on Mars that is thought to be either permafrost ground or vesicular basalt ($\Phi \approx 30\%$). The authors discussed whether it is more appropriate to model vesicular basalt as a low cohesive soil (dry sand scaling) with the effective strength of a rock or as a low-porosity rock with reduced strength (due to the reduced crater efficiency caused by porosity). A comparison of the crater scaling relationships results in 50% larger craters in the latter case, which affects the interpretation of surface ages when those two different units are compared.

In contrast, our findings demonstrate that the coefficient of friction, cohesion, and porosity do not only influence the effective strength but also strongly affect the scaling parameters. For instance, we have demonstrated that the transient crater diameter at which the strength-to-gravity transition occurs changes with different target properties (Figure 6). Moreover, our results show that cratering scaling relationships for wet soils are only appropriate for nonporous and low coefficient of friction targets but expected to be different for targets with coefficients of friction similar to dry sands or rocks. We also

pointed out that the effective strength is somewhat related to the cohesion Y_0, because a strength regime is only observable for cases where $Y_0 \neq 0$. The strength term in crater scaling relationship Y_{EFF} seems to be about ~21 times larger than the strength parameter used in our numerical models, Y_0. The relationship is depicted in section 5.3, however, only for target properties for weak low-strength materials ($10\% \leq \Phi \leq 20\%$, $0.6 \leq f \leq 0.8$), because the compaction parameters may become important for lower porosity.

We emphasize that accurate information on target properties is crucial in order to use these crater scaling relationships appropriately. The estimation of target properties at smaller scales on planetary bodies other than Earth is complicated, mainly because one needs to guess the geological setting from the morphology, site resurfacing history, and terrestrial rock analogues. Furthermore, the effective strength and other scaling parameters should ideally be varied accordingly, because changes in target properties are likely accompanied by changes in other properties. In other words, we expect an increase in porosity to be accompanied with a decrease in target strength (i.e., coefficient of friction and cohesion). Additional challenges arise from target layering due to volcanism, erosion, the presence of volatiles [e.g., *Kieffer and Simonds*, 1980], thermal evolution [e.g., *Miljković et al*., 2013], and the differences in mechanical and physical properties at laboratory and planetary scales [e.g., *Grady and Kipp*, 1980]. Further complexity is induced by the temporal and spatial variations associated with some of these factors, e.g., the observed density and porosity variations across the lunar surface [*Wieczorek et al*., 2013] and the decrease of porosity with depth due to the increasing lithostatic pressure [e.g., *Han et al*., 2014; *Milbury et al*., 2015; *Soderblom et al*., 2015]. Moreover, target heterogeneities may have strong effects on small scales, but not on larger scales, or vice versa [Cooper, 1977]. This demonstrates the need for additional constraints on target property variations on planetary bodies, in particular the effective target strength at large scales (i.e., meters to kilometers). Accurate estimates of physical and mechanical properties on planetary surfaces are crucial for the development of reliable model parametrizations and thus for dating planetary surfaces with different target properties. Ideally, a combination of several techniques (like gravity, topography, spectroscopy, and photo geology) should be used to constrain such properties, e.g., the porosity of the lunar shallow crust [*Huang and Wieczorek*, 2012].

8. Conclusions

A simple numerical model setup has been developed to investigate the effect of target properties on the transient crater diameter in simple crater formation. Under the simplifications made in our approach, our numerical results show this setup to reproduce transient crater diameters for simple craters within ±5% for water, low-strength and low-porosity targets (e.g., wet sand), and targets with weak low strength and moderate porosity ($>$ 10–15%) such as sands. For less porous and harder targets, the influence of compaction parameters on the transient crater diameter scaling may not be negligible and results might be less robust. With our modeling we have derived crater scaling relationships for 90 new combinations of coefficient of friction and porosity, filling a gap in the amount of existing transient crater diameter relationships. Simulation results predict that both porosity and friction coefficient have a large influence on the shape of the transient cavity and correspondingly derived empirical relationships. For porosities lower than 30%, the velocity-scaling exponent μ reflects the reduction in crater efficiency induced by the coefficient of friction, while the scaling coefficient K_D reflects the porosity-induced reduction in crater efficiency. Using these two observations, we have incorporated the effect of the coefficient of friction and porosity in crater scaling laws and reproduced transient crater diameters within ±5% if compared to cases where no assumptions are made. At larger porosities, our data may suggest an increase in the penetration depth, which affects the derived scaling parameter μ and makes it more difficult to incorporate target properties directly in crater scaling laws. Based on simulations for cohesive materials, we have found the strength term in the crater scaling laws (i.e., the effective strength) to be dependent on target properties and to be ~21 times larger than the cohesion in our numerical models, which opens the possibility to relate target strength in numerical models to natural targets. Our new crater scaling relationships and equations have been derived for lunar conditions and allow to calculate transient crater diameters for varying target properties across geological units on the lunar surface. Further study is required to fully understand the effect of varying impact velocities on crater scaling laws and to answer the question whether our crater relationships are applicable on other planetary bodies.

Acknowledgments
We are grateful to G.S. Collins, B.A. Ivanov, and K. Miljković for their constructive comments, which improved this paper. N.C.P., T.R., Z.X., and S.C.W. appreciate the support by the Research Council of Norway via the 235058/F20 CRATER CLOCK grant and a Centre of Excellence grant to the Centre of Earth Evolution and Dynamics (CEED, 223272) as well as the IS-DAAD mobility grant (NFR 244761/F11). K.W. and R.L. are supported by the IS-DAAD mobility grant 57159947. K.W. and R.L. are funded by the DFG grants MEMIN FOR887, WU 355/6-2, and SFB-TRR 170 (A4), Pub.#21. All calculations have been performed on STALLO, a Notur high-performance computing facility at the University of Tromsø under project IDs nn9283 and nn9010. We would also like to acknowledge the developers of iSALE and pySALEplot (G.S. Collins, K. Wünnemann, D. Elbeshausen, B.A. Ivanov, H.J. Melosh, and T. Davison). Details regarding iSALE are available at www.isale-code.de. Supporting information can be found in the online version.

References

Amsden, A. A., H. M. Ruppel, and C. W. Hirt (1980), SALE: A simplified ALE computer program for fluid flow at all speeds, US Department of Commerce, National Technical Information Service.

Buckingham, E. (1914), On physically similar systems; illustrations of the use of dimensional equations, *Phys. Rev.*, *4*(4), 345.

Cintala, M. J., C. A. Wood, and J. W. Head (1977), The effects of target characteristics on fresh crater morphology—Preliminary results for the Moon and Mercury, paper presented at 8th Lunar and Planetary Science Conference Proceedings, 3409–3425.

Collins, G. S. (2014), Numerical simulations of impact crater formation with dilatancy, *J. Geophys. Res. Planets*, *119*, 2600–2619, doi:10.1002/2014JE004708.

Collins, G. S., H. J. Melosh, and B. A. Ivanov (2004), Modeling damage and deformation in impact simulations, *Meteorit. Planet. Sci.*, *39*(2), 217–231, doi:10.1111/j.1945-5100.2004.tb00337.x.

Collins, G. S., H. J. Melosh, and R. A. Marcus (2005), Earth Impact Effects Program: A Web-based computer program for calculating the regional environmental consequences of a meteoroid impact on Earth, *Meteorit. Planet. Sci.*, *40*(6), 817–840, doi:10.1111/j.1945-5100.2005.tb00157.x.

Collins, G. S., H. J. Melosh, and K. Wünnemann (2011), Improvements to the ε-α porous compaction model for simulating impacts into high-porosity solar system objects, *Int. J. Impact Eng.*, *38*(6), 434–439, doi:10.1016/j.ijimpeng.2010.10.013.

Cooper, H. F., Jr. (1977), A summary of explosion cratering phenomena relevant to meteor impact events, paper presented at Impact and Explosion Cratering: Planetary and Terrestrial Implications; Proceedings of the Symposium on Planetary Cratering Mechanics, Flagstaff, Ariz., September 13–17, 1976. (A78–44030 19–91), Pergamon Press, New York.

Croft, S. K. (1985), The scaling of complex craters, *J. Geophys. Res.*, *90*(S02), C828–C842, doi:10.1029/JB090iS02p0C828.

Davison, T. M., G. S. Collins, and P. A. Bland (2016), Mesoscale modeling of impact compaction of primitive solar system solids, *Astrophys. J.*, *821*(1), 68, doi:10.3847/0004-637X/821/1/68.

Davison, T. M., G. S. Collins, and F. J. Ciesla (2010), Numerical modelling of heating in porous planetesimal collisions, *Icarus*, *208*(1), 468–481, doi:10.1016/j.icarus.2010.01.034.

Davison, T. M., G. S. Collins, D. Elbeshausen, K. Wünnemann, and A. Kearsley (2011), Numerical modeling of oblique hypervelocity impacts on strong ductile targets, *Meteorit. Planet. Sci.*, *46*(10), 1510–1524, doi:10.1111/j.1945-5100.2011.01246.x.

Dence, M. R. (1968), Shock zoning at Canadian craters: Petrography and structural implications, in *Shock Metamorphism of Natural Materials*, edited B. M. French and N. M. Short, pp. 169–184, Mono Book Corp., Baltimore, Md.

Dienes, J. K., and J. M. Walsh (1970), Theory of impact: Some general principles and the method of Eulerian codes, in *High-Velocity Impact Phenomena*, edited R. Kinslow, pp. 46–104, Academic Press, New York.

Dundas, C. M., L. P. Keszthelyi, V. J. Bray, and A. S. McEwen (2010), Role of material properties in the cratering record of young platy-ridged lava on Mars, *Geophys. Res. Lett.*, *37*, L12203, doi:10.1029/2010GL042869.

Elbeshausen, D., K. Wünnemann, and G. S. Collins (2009), Scaling of oblique impacts in frictional targets: Implications for crater size and formation mechanisms, *Icarus*, *204*(2), 716–731, doi:10.1016/j.icarus.2009.07.018.

Fassett, C. I. (2016), Analysis of impact crater populations and the geochronology of planetary surfaces in the inner solar system, *J. Geophys. Res. Planets*, *121*, 1900–1926, doi:10.1002/2016JE005094.

Gault, D. E. (1973), Displaced mass, depth, diameter, and effects of oblique trajectories for impact craters formed in dense crystalline rocks, *Earth Moon Planet.*, *6*(1), 32–44, doi:10.1007/BF02630651.

Gault, D. E., and C. P. Sonett (1982), Laboratory simulation of pelagic asteroidal impact: Atmospheric injection, benthic topography, and the surface wave radiation field, *Geol. Soc. Am. Spec. Pap.*, *190*, 69–92, doi:10.1130/SPE190-p69.

Gault, D. E., and J. A. Wedekind (1977), Experimental hypervelocity impact into quartz sand—II: Effects of gravitational acceleration, paper presented at Impact and Explosion Cratering: Planetary and Terrestrial Implications; Proceedings of the Symposium on Planetary Cratering Mechanics, Flagstaff, Ariz., September 13–17, 1976. (A78–44030 19–91), Pergamon Press, New York.

Grady, D. E., and M. E. Kipp (1980), Continuum modelling of explosive fracture in oil shale, paper presented at International Journal of Rock Mechanics and Mining Sciences & Geomechanics Abstracts, Elsevier.

Grieve, R., and J. Garvin (1984), A geometric model for excavation and modification at terrestrial simple impact craters, *J. Geophys. Res.*, *89*(B13), 11561–11572, doi:10.1029/JB089iB13p11561.

Güldemeister, N., K. Wünnemann, N. Durr, and S. Hiermaier (2013), Propagation of impact-induced shock waves in porous sandstone using mesoscale modeling, *Meteorit. Planet. Sci.*, *48*(1), 115–133, doi:10.1111/j.1945-5100.2012.01430.x.

Güldemeister, N., K. Wünnemann, and M. Poelchau (2015), Scaling impact crater dimensions in cohesive rock by numerical modeling and laboratory experiments, *Geol. Soc. Am. Spec. Pap.*, *518*, SPE518–SPE502, doi:10.1130/2015.2518(02).

Han, S. C., N. Schmerr, G. Neumann, and S. Holmes (2014), Global characteristics of porosity and density stratification within the lunar crust from GRAIL gravity and Lunar Orbiter Laser Altimeter topography data, *Geophys. Res. Lett.*, *41*, 1882–1889, doi:10.1002/2014GL059378.

Holsapple, K. A. (1993), The scaling of impact processes in planetary sciences, *Annu. Rev. Earth Planet. Sci.*, *21*(1), 333–373, doi:10.1146/annurev.ea.21.050193.002001.

Holsapple, K. A., and K. R. Housen (2007), A crater and its ejecta: An interpretation of deep impact, *Icarus*, *191*(2), 586–597, doi:10.1016/j.icarus.2006.08.035.

Holsapple, K. A., and K. R. Housen (2017), Craters from impacts and explosion. [Available at http://keith.aa.washington.edu/craterdata/scaling/theory.pdf, Accessed February 08, 2017.]

Holsapple, K. A., and R. M. Schmidt (1979), A material-strength model for apparent crater volume, paper presented at 10th Lunar and Planetary Science Conference Proceedings

Holsapple, K. A., and R. M. Schmidt (1982), On the scaling of crater dimensions 2. Impact processes, *J. Geophys. Res.*, *87*(B3), 1849–1870, doi:10.1029/JB087iB03p01849.

Holsapple, K. A., and R. M. Schmidt (1987), Point source solutions and coupling parameters in cratering mechanics, *J. Geophys. Res.*, *92*(B7), 6350–6376, doi:10.1029/JB092iB07p06350.

Housen, K. R. (1999), Scale effects in strength-dominated collisions of rocky asteroids, *Icarus*, *142*(1), 21–33, doi:10.1006/icar.1999.6206.

Housen, K. R., and K. A. Holsapple (2003), Impact cratering on porous asteroids, *Icarus*, *163*(1), 102–119, doi:10.1016/s0019-1035(03)00024-1.

Housen, K. R., and K. A. Holsapple (2011), Ejecta from impact craters, *Icarus*, *211*, 856–875, doi:10.1029/JB087iB03p01849.

Huang, Q., and M. A. Wieczorek (2012), Density and porosity of the lunar crust from gravity and topography, *J. Geophys. Res.*, *117*, E05003, doi:10.1029/2012JE004062.

Ivanov, B. A. (2001), Mars/Moon cratering rate ratio estimates, *Space Sci. Rev.*, *96*(1), 87–104, doi:10.1023/A:1011941121102.

Ivanov, B. A., D. Deniem, and G. Neukum (1997), Implementation of dynamic strength models into 2D hydrocodes: Applications for atmospheric breakup and impact cratering, *Int. J. Impact Eng.*, *20*(1–5), 411–430, doi:10.1016/s0734-743x(97)87511-2.

Kadono, T. (1999), Hypervelocity impact into low density material and cometary outburst, *Planet. Space Sci.*, *47*(3), 305–318, doi:10.1016/S0032-0633(98)00039-7.
Kadono, T., and A. Fujiwara (2005), Cavity and crater depth in hypervelocity impact, *Int. J. Impact Eng.*, *31*(10), 1309–1317, doi:10.1016/j.ijimpeng.2004.08.003.
Kiefer, W. S., R. J. Macke, D. T. Britt, A. J. Irving, and G. J. Consolmagno (2012), The density and porosity of lunar rocks, *Geophys. Res. Lett.*, *39*, L07201, doi:10.1029/2012GL051319.
Kieffer, S. W. (1975), From regolith to rock by shock, *Earth Moon Planet.*, *13*(1), 301–320, doi:10.1007/BF00567522.
Kieffer, S. W., and C. H. Simonds (1980), The role of volatiles and lithology in the impact cratering process, *Rev. Geophys.*, *18*(1), 143–181, doi:10.1029/RG018i001p00143.
Love, S. G., F. Hörz, and D. E. Brownlee (1993), Target porosity effects in impact cratering and collisional disruption, *Icarus*, *105*(1), 216–224, doi:10.1006/icar.1993.1119.
Luther, R., N. Artemieva, M. Ivanova, C. Lorenz, and K. Wünnemann (2017), Snow carrots after the Chelyabinsk event and model implications for highly porous solar system objects, *Meteorit. Planet. Sci.*, *52*(5), 979–999, doi:10.1111/maps.12831.
Marchi, S., M. Massironi, G. Cremonese, E. Martellato, L. Giacomini, and L. Prockter (2011), The effects of the target material properties and layering on the crater chronology: The case of Raditladi and Rachmaninoff basins on Mercury, *Planet. Space Sci.*, *59*(15), 1968–1980, doi:10.1016/j.pss.2011.06.007.
Melosh, H., and B. Ivanov (1999), Impact crater collapse, *Annu. Rev. Earth Planet. Sci.*, *27*(1), 385–415.
Melosh, H. J. (1989), *Impact Cratering: A Geologic Process*, *Oxford Monographs on Geology and Geophysics, No. 11*, p. 253 pp., Research supported by NASA , Oxford University Press, New York.
Melosh, H. J. (2007), A hydrocode equation of state for SiO_2, *Meteorit. Planet. Sci.*, *42*(12), 2079–2098, doi:10.1111/j.1945-5100.2007.tb01009.x.
Melosh, H. J., E. V. Ryan, and E. Asphaug (1992), Dynamic fragmentation in impacts: Hydrocode simulation of laboratory impacts, *J. Geophys. Res.*, *97*(E9), 14,735–14,759, doi:10.1029/92JE01632.
Milbury, C., B. C. Johnson, H. J. Melosh, G. S. Collins, D. M. Blair, J. M. Soderblom, F. Nimmo, C. J. Bierson, R. J. Phillips, and M. T. Zuber (2015), Preimpact porosity controls the gravity signature of lunar craters, *Geophys. Res. Lett.*, *42*, 9711–9716, doi:10.1002/2015GL066198.
Miljković, K., G. S. Collins, D. J. Chapman, M. R. Patel, and W. Proud (2012), High-velocity impacts in porous solar system materials, paper presented at AIP Conference Proceedings.
Miljković, K., M. A. Wieczorek, G. S. Collins, M. Laneuville, G. A. Neumann, H. J. Melosh, S. C. Solomon, R. J. Phillips, D. E. Smith, and M. T. Zuber (2013), Asymmetric distribution of lunar impact basins caused by variations in target properties, *Science*, *342*(6159), 724–726, doi:10.1126/science.1243224.
Moore, H. J., D. E. Gault, and R. V. Lugn (1963), Experimental impact craters in basalt, *Trans. Min. Eng*, *229*, 258–262.
Neukum, G., and B. Ivanov (1994), Crater size distributions and impact probabilities on Earth from lunar, terrestrial-planet, and asteroid cratering data, in *Hazards Due to Comets and Asteroids*, edited by T. Gehrels, pp. 359–416, Univ. Arizona Press, Tucson.
O'Keefe, J. D., and T. J. Ahrens (1993), Planetary cratering mechanics, *J. Geophys. Res.*, *98*(E9), 17011–17028, doi:10.1029/93JE01330.
Ohnaka, M. (1995), A shear failure strength law of rock in the brittle-plastic transition regime, *Geophys. Res. Lett.*, *22*(1), 25–28, doi:10.1029/94GL02791.
Ormö, J., I. Melero-Asensio, K. R. Housen, K. Wünnemann, D. Elbeshausen, and G. S. Collins (2015), Scaling and reproducibility of craters produced at the Experimental Projectile Impact Chamber (EPIC), Centro de Astrobiología, Spain, *Meteorit. Planet. Sci.*, *50*(12), 2067–2086, doi:10.1111/maps.12560.
Piekutowski, A. J. (1977), Cratering mechanisms observed in laboratory-scale high-explosive experiments, paper presented at Impact and Explosion Cratering: Planetary and Terrestrial Implications; Proceedings of the Symposium on Planetary Cratering Mechanics, Flagstaff, Ariz., September 13–17, 1976. (A78–44030 19–91), pp. 67–102, Pergamon Press, New York.
Pierazzo, E. (1997), A reevaluation of impact melt production, *Icarus*, *127*(2), 408–423, doi:10.1006/icar.1997.5713.
Pierazzo, E., N. Artemieva, E. Asphaug, E. C. Baldwin, J. Cazamias, R. Coker, G. S. Collins, D. A. Crawford, T. M. Davison, and D. Elbeshausen (2008), Validation of numerical codes for impact and explosion cratering: Impacts on strengthless and metal targets, *Meteorit. Planet. Sci.*, *43*(12), 1917–1938, doi:10.1111/j.1945-5100.2008.tb00653.x.
Pierazzo, E., N. Artemieva, and B. Ivanov (2005), Starting conditions for hydrothermal systems underneath Martian craters: Hydrocode modeling, *Geol. Soc. Am. Spec. Pap.*, *384*, 443–457, doi:10.1130/0-8137-2384-1.443.
Pierazzo, E., and G. S. Collins (2004), A brief introduction to hydrocode modeling of impact cratering, in *Cratering in Marine Environments and on Ice*, edited H. Dypvik and M. J. Burchell, pp. 323–340, Springer, New York.
Pike, R. J. (1980), Control of crater morphology by gravity and target type—Mars, Earth, Moon, paper presented at 11th Lunar and Planetary Science Conference Proceedings, 2159–2189.
Poelchau, M. H., T. Kenkmann, K. Thoma, T. Hoerth, A. Dufresne, and F. Schäfer (2013), The MEMIN research unit: Scaling impact cratering experiments in porous sandstones, *Meteorit. Planet. Sci.*, *48*(1), 8–22, doi:10.1111/maps.12016.
Richardson, J. E. (2009), Cratering saturation and equilibrium: A new model looks at an old problem, *Icarus*, *204*(2), 697–715, doi:10.1016/j.icarus.2009.07.029.
Robbins, S. J., and B. M. Hynek (2012), A new global database of Mars impact craters ≥1 km: 2. Global crater properties and regional variations of the simple-to-complex transition diameter, *J. Geophys. Res.*, *117*, E06001, doi:10.1029/2011JE003967.
Schmidt, R. M. (1980), Meteor crater: Energy of formation—Implications of centrifuge scaling, 2099–2128, paper presented at 11th Lunar and Planetary Science Conference Proceedings.
Schmidt, R. M., K. A. Holsapple, and K. R. Housen (1986), Gravity effects in cratering, Report DNA-TR-86–182, Defense Nuclear Agency, Washington, D. C.
Schmidt, R. M., and K. R. Housen (1987), Some recent advances in the scaling of impact and explosion cratering, *Int. J. Impact Eng.*, *5*(1), 543–560, doi:10.1016/0734-743X(87)90069-8.
Schultz, P. H., and J. Spencer (1979), Effects of substrate strength on crater statistics: Implications for surface ages and gravity scaling, 1081–1083, paper presented at 10th Lunar and Planetary Science Conference.
Slyuta, E. (2014), Physical and mechanical properties of the lunar soil (a review), *Sol. Syst. Res.*, *48*(5), 330–353.
Soderblom, J. M., A. J. Evans, B. C. Johnson, H. J. Melosh, K. Miljković, R. J. Phillips, J. C. Andrews-Hanna, C. J. Bierson, J. W. Head, and C. Milbury (2015), The fractured Moon: Production and saturation of porosity in the lunar highlands from impact cratering, *Geophys. Res. Lett.*, *42*, 6939–6944, doi:10.1002/2015GL065022.
Turtle, E. P., E. Pierazzo, G. S. Collins, G. R. Osinski, H. J. Melosh, J. V. Morgan, and W. U. Reimold (2005), Impact structures: What does crater diameter mean?, *Geol. Soc. Am. Spec. Pap.*, *384*, 1–24, doi:10.1130/0-8137-2384-1.1.

Vajdova, V., P. Baud, and T. F. Wong (2004), Compaction, dilatancy, and failure in porous carbonate rocks, *J. Geophys. Res.*, *109*, B05204, doi:10.1029/2003JB002508.

van der Bogert, C. H., H. Hiesinger, C. M. Dundas, T. Krüger, A. S. McEwen, M. Zanetti, and M. S. Robinson (2016), Origin of discrepancies between crater size-frequency distributions of coeval lunar geologic units via target property contrasts, *Icarus*, doi:10.1029/2003JB002508.

Werner, S. C., and B. A. Ivanov (2015), Exogenic dynamics, cratering and surface ages, in *Treatise on Geophysics*, 2nd ed., vol. 11, edited G. Schubert, pp. 327–365, Elsevier, Amsterdam.

Wieczorek, M. A., et al. (2013), The crust of the Moon as seen by GRAIL, *Science*, *339*(6120), 671–675, doi:10.1126/science.1231530.

Wong, T., and P. Baud (1999), Mechanical compaction of porous sandstone, *Oil Gas Sci. Technol.*, *54*(6), 715–727, doi:10.2516/ogst:1999061.

Wood, C., and L. Anderson (1978), New morphometric data for fresh lunar craters, paper presented at 9th Lunar and Planetary Science Conference Proceedings.

Wünnemann, K., G. S. Collins, and H. J. Melosh (2006), A strain-based porosity model for use in hydrocode simulations of impacts and implications for transient crater growth in porous targets, *Icarus*, *180*(2), 514–527, doi:10.1016/j.icarus.2005.10.013.

Wünnemann, K., G. S. Collins, and G. R. Osinski (2008), Numerical modelling of impact melt production in porous rocks, *Earth Planet. Sci. Lett.*, *269*(3–4), 530–539, doi:10.1016/j.epsl.2008.03.007.

Wünnemann, K., D. Nowka, G. S. Collins, D. Elbeshausen, and M. Bierhaus (2011), Scaling of impact crater formation on planetary surfaces: Insights from numerical modeling, in *Proceedings of the 11th Hypervelocity Impact Symposium*, *Freiburg*.

Wünnemann, K., M. H. Zhu, and D. Stöffler (2016), Impacts into quartz sand: Crater formation, shock metamorphism, and ejecta distribution in laboratory experiments and numerical models, *Meteorit. Planet. Sci.*, *51*(10), 1762–1794, doi:10.1111/maps.12710.

Yamamoto, S., S. Hasegawa, A. Suzuki, and T. Matsunaga (2017), Impact velocity dependence of transient cratering growth, *J. Geophys. Res. Planets*, *122*, 1077–1089, doi:10.1002/2016JE005252.

Yamamoto, S., K. Wada, N. Okabe, and T. Matsui (2006), Transient crater growth in granular targets: An experimental study of low velocity impacts into glass sphere targets, *Icarus*, *183*(1), 215–224, doi:10.1016/j.icarus.2006.02.002.

Zel'Dovich, Y. B., and Y. P. Raizer (1966), *Physics of Shock Waves and High Temperature Phenomena*, vol. 1, pp. 839–846, Academic Press, New York.